ELECTRICAL CONDUCTIVITY AND RELATED DEFECT STRUCTURES IN REDUCED RUTILE

Tae Il Oh
B.S. Physics, Seoul National University, 1964
M.S. Materials Science, University of Utah, 1977
M.S. Ceramic Science, Ohio State University, 1979

A dissertation submitted to the faculty
of the Oregon Graduate Center
in partial fulfillment of the
requirements for the degree
Doctor of Philosophy
in
Materials Science
September, 1985

The dissertation "Electrical Conductivity and Related Defect Structures in Reduced Rutile" by Tae Il Oh has been examined and approved by the following Examination Committee:

Nicholas G. Eror, Thesis Advisor
Professor

Jack H. Devletian
Associate Professor

Wallace B. Leigh
Assistant Professor

Robert M. Drosd
Adjunct Assistant Professor

ACKNOWLEDGEMENT

I would like to express special thanks to professor Nicholas G. Eror for his continuous advice and encouragement, professor John S. Blakemore for valuable discussions and the members of thesis committee, Dr. Jack H. Devletian, Dr. Wallace B. Leigh, and Dr. Robert Drosd for reviewing this dissertation. Thanks are also due to the Department of Materials Science and Engineering for the use of the facilities during this work.

I also thank my colleague for discussions, especially Dr. U. Balachandran with experimental process, and Mr. Kun K. Ryoo with T.E.M. work.

I would like to acknowledge the financial support by Gas Research Institute for this work.

Finally I dedicate this accomplishment to my family, without whose love and support this would not have been possible.

TABLE OF CONTENTS

LIST OF TABLES

LIST OF FIGURES

ABSTRACT

Electrical conductivity and related defect structures in reduced rutile

Tae Il Oh, Ph.D.
Oregon Graduate Center, 1985

Supervising Professor: Nicholas G. Eror

Stoichiometric TiO_2, rutile is an insulator at room temperature, while reduced nonstoichiometric rutile is semiconductive. The electrical properties of nonstoichiometric rutile depend on its defect structure. Reduced rutile is characterized as two groups; a homologous series of phases of Ti_nO_{2n-1} and nonstoichiometric TiO_{2-x}.

In the homologous series of phases, defective crystallographic shear planes(CS planes) are so regular in the rutile structure that a superlattice structure is generated. Before the homologous phases are produced, the state of the reduced crystal is that of the point defect or irregular extended defect state which is expressed as $TiO_{2-x}(x<<1)$.

The electrical conductivity measurements of undoped and doped rutile at thermodynamic equilibrium with controlled oxygen activities have been conducted and interpreted in terms of corresponding defects within TiO_{2-x}.
In very low oxygen activity, an anomalous dependence

of conductivity is observed. The conventional point defect model cannot explain this behavior.

A new reaction model is derived to interpret the observed results and microstructure analysis under T.E.M. supports the modified model for its application to the phenomenological results at very low oxygen activities.

1. INTRODUCTION

Properties of materials such as mechanical, thermal, and electrical, are related to the internal structure which always tends to be imperfect for temperature above absolute zero. These imperfections in crystals change the characteristics of these properties.

The types of imperfections are classified as point and extended defects. Point defects include atomic disorder such as vacant lattice sites, interstitials, antistructure, foreign atoms, and electronic disorder. Extended defects are defect clusters such as line defects(dislocations) and planar defects.

The control of defect concentrations in crystals is of prime importance in determining their properties. This has been explored by a statistical thermodynamic approach.(1)

In an elemental crystal, possible defects are vacant lattice site, interstitials including their ionized states and electronic defects. When a foreign atom is contained in a crystal, it occupies the lattice substitutionally or resides at an interstitial site. The solubility of a foreign atom depends on the influence between the foreign atom and native defects through association (e.g.($V_m F_m$)) and electrical neutrality condition; i.e.in general

imperfections with charges of opposite sign increase their respective solubilities while imperfections with charges of the same sign decrease their respective solubilities.

For a pure compound, the atomic imperfections are distinguished as Frenkel, Schottky-Wagner and antistructure disorder. Associations consisting of a pair of two compensating imperfections are also possible.

Atomic disorder can lead to an excess or deficit of one of the components resulting in a nonstoichiometric compound. The ratio of cation/anion can be controlled by equilibration under the controlled atmosphere of one constituent of the compound. Another way of controlling the cation/anion ratio is to dope aliovalent atoms into a crystal. The occupation of foreign atoms on particular lattice sites depends on electronegativity and size factors. (1)

With the increase of defect concentration the lattice potential energy increases and the crystal becomes unstable. As a result a new composition or crystal structure is generated. Therefore, there is a limited extent of solubility of native defects or foreign atoms in a crystal.
The defect structure model is derived from experimental data such as electrical property measurement,(2-9) thermo-

gravimetry, (10-14) diffusion coefficient measurement,(15,16) optical(17) and ESR techniques.(18-20) One of the interesting defect structures is that of a crystallographic shear plane (CS plane) for extended defects which are commonly observed in nonstoichiometric transition metal oxides.(21) One of the most intensively studied phase showing this class of disorder is TiO_{2-x}, where there is still disagreement as to defect specie with and without the CS plane extended defect, as well as how the electrical behavior is related to the defect model. This study investigated the defect structures of reduced rutile for both undoped and doped conditions at high temperature and correlated the observed conductivity behavior with the proper defect reaction model.

2.REVIEW OF RELATED WORK

Deviations from the stoichiometric composition in transition metal oxides and oxide compounds have been determined by electrochemical cells, thermogravimetric analysis, or electrical conductivity measurement. Most investigations have been carried out by thermogravimetric and electrical conductivity measurements.

2-1.Electrical conductivity measurement.

Metal excess rutile in a reducing atmosphere can be described by the generation of oxygen vacancies or titanium interstitials which may be ionized in several states. Possible types of defect structures can be derived from the dependence of electrical conductivity in various ranges of anion activity. But this dependence does not necessarily indicate unique type of defect structure because different types of defect may give the same or similar slopes of conductivity dependence. Despite this ambiguity, the electrical conductivity measurement is a common way for determining the defect structure in a high temperature environment.

Blumenthal et al(4) measured conductivity of single crystals over the temperature range of 1000°C- 1500°C and oxygen pressures of 1- 10^{-15} atmospheres. In this experimental range, the nonstoichiometric rutile is classified as a metal excess, n-type semiconductor. The qualitative observations were that at high temperature the slope of log conductivity vs log P_{O_2} was close to -1/5 throughout the experimental pressure range at high temperature, and close to -1/5.6 with lowering temperature at high oxygen partial pressures, but close to -1/4 at low oxygen pressures. Based on this result they concluded that the dominant lattice defects were tri- and tetravalent titanium interstitials and donor impurities.

Marucco et al(10) investigated the reduction of TiO_2 at 800°C - 1100°C by means of thermogavimetric and electrical conductivity measurements. They observed three different slopes of dependence, -1/5 at high temperature and low pressure, -1/6 at low temperature and low pressure,and -1/4 at low temperature and high pressure. The predominant defects were analysed as tetravalent titanium interstitials for the -1/5 dependence, divalent oxygen vacancies for the -1/6 dependence, and monovalent oxygen vacancies for the -1/4 dependence. They insisted that singly ionized native oxygen vacancies rather than acceptor impurities

for the -1/4 dependence were dominant defects because two samples from different sources showed the same result. But generally, impurity effects at high pressure and low temperature can hardly be neglected. Assuming the acceptor impurity effect, doubly ionized oxygen vacancies lead to the -1/4 slope. They noticed that the mobility of electrons is independent of the concentration and nature of the defect at a fixed temperature.
Baumard et al(22) studied the Ti-O system between Ti_3O_5 and TiO_2 by electrical conductivity measurements as a function of oxygen partial pressure at high temperatures. The experimental range of observation extended beyond the region observed by other investigators mentioned previously. Further reduction beyond the -1/5 slope region, where defects were attributed to tetravalent titanium interstitials, showed an abrupt increase in conductivity. They attributed this behavior to the occurrence of extended defects of crystallographic shear planes.
It has been known that in some transition metal oxides such as Ti, Nb, and W, considerable deviation from stoichiometry creates some degree of CS planes to accomodate vacancies or interstitials.(21)

Doping with aliovalent cations changes the physical properties of materials. Cr-doped rutile showed that

the conductivity dependence shifted toward lower pressure compared to that of undoped samples. Therefore,the increase of acceptor dopant concentration moves the p-n transition region to lower pressures. Ta-doped rutile showed -1/5, 0, and -1/4 slopes respectively from lower to higher oxygen pressures. The predominant defects for each region were analysed as titanium interstitials, excess electrons, and metal vacancies based on a point defect model.(3,6,23)

2-2. Thermogravimetric measurement.

The variation of oxygen content in rutile equilibrated with temperature and oxygen pressure has been studied by weight change measurements. From the relation between the change of oxygen content and electrical neutrality conditions, it is possible to obtain the equilibrium defect structure.

Førland observed that the weight loss was proportional to $P_{O_2}^{-1/6}$ at temperatures above 1100°C and $10^{-7} > P_{O_2} > 10^{-16}$atm. The defects in the range were concluded to be doubly ionized oxygen vacancies.(24)

Rosa et al(25) observed the weight change of TiO_{2-x} in the reducing atmosphere of CO/CO_2 mixtures where

$10^{-12} > P_{O_2} > 10^{-18}$ bar at 1273°K, was proportional to $P_{O_2}^{-1/4.81}$ and suggested that defects consisted of tri- and tetravalent titanium interstitials. They also investigated the solid solution of TiO_2 with 0.1-3 mole % of Nb_2O_5 at 1273°K.(13) The sample containing less than 1 mole % Nb_2O_5 was concluded to consist of titanium interstitials for $10^{-18} < P_{O_2} < 10^{-12}$ bar.
Merritt et al and Bursill et al(11) studied the thermodynamics of the Ti-O system from Ti_3O_5 to TiO_2 at 1304°K. Even in the very slightly reduced rutile, TiO_x with $x > 1.98$, they found extended defect CS planes. There is still no agreement on the extent of nonstoichiometry with the presence of point defects.

2-3. Structure of nonstoichiometric rutile.

The Ti-O binary system of the phase diagram is shown in Fig.1. Between stoichiometric rutile and monoclinic Ti_3O_5, both a wide range of a homologous series of oxides with the composition Ti_nO_{2n-1} and a narrow range of slight deviation from stoichiometry where the deviation is accommodated by point defects or their associations exist. The interesting range in this investigation is the transition from the point defect to the homologous series region.

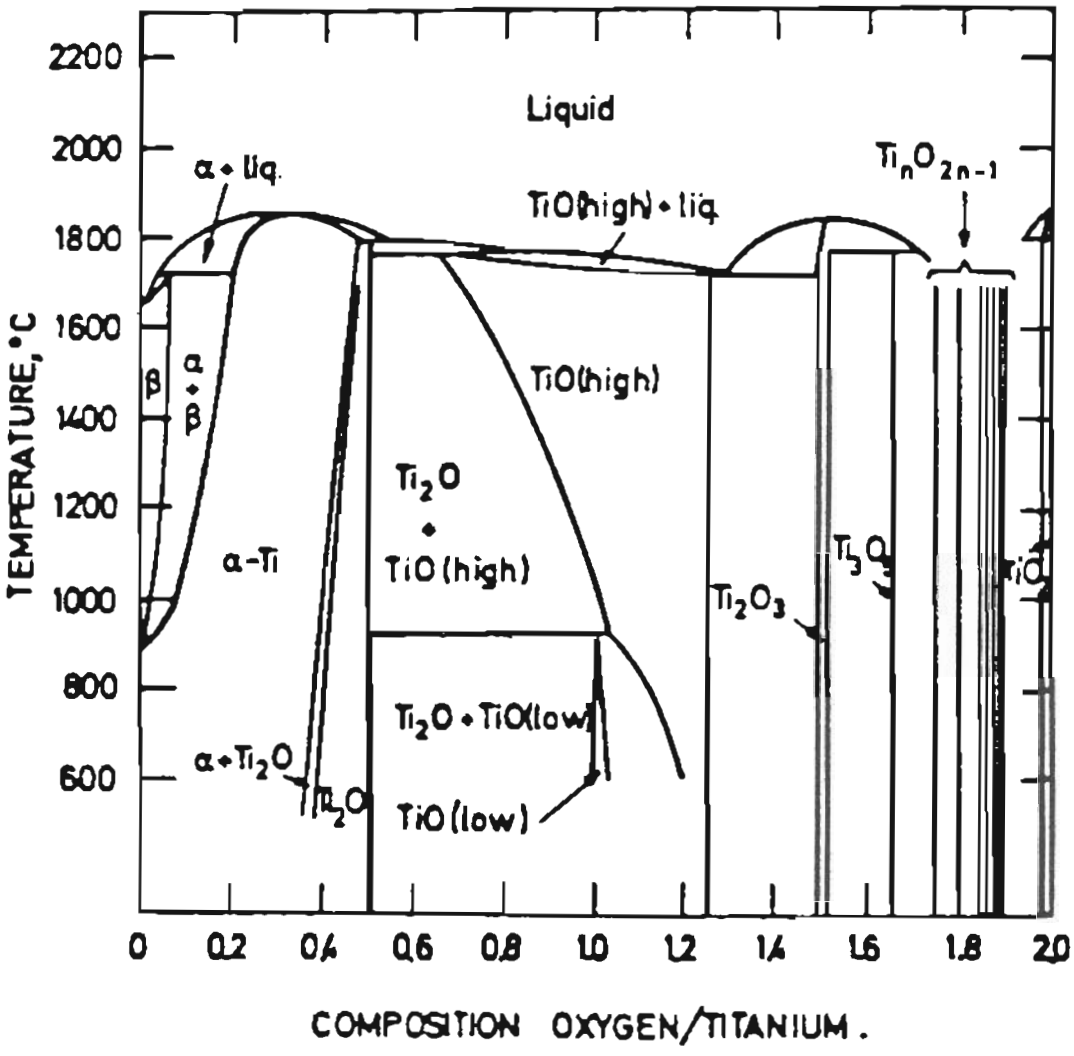

Fig. 1. Ti-O phase diagram.

(1). Structure of stoichiometric rutile.

The highest oxide, TiO_2, has polymorphic phases of rutile,anatase, brookite, and alpa-PbO_2 type structure. At one atmosphere rutile is the most stable phase and will only be considered further. Its structure consists of rectilinear ribbons of edge-shared TiO_6-octahedra joined by corner-sharing to similar ribbons so that the orientations of adjacent ribbons differ by 90 degrees. The unit cell is tetragonal (Fig.2). Projection along the b axis suggests that the oxygen arrangement is approximately h.c.p.(Fig.3a). The oxygen layers are slightly puckered by projection along the c axis, but a small topological distortion generates an idealized h.c.p.anion arrangement. The titanium atoms fill alternate rows of octahedral interstices parallel to c axis. An idealized (010) layer is shown in Fig.3a.

(2). Structure of reduced rutile.

In reduced rutile there are three characterized regions,i.e.the regions of dominant point defects, random CS planes with point defects, and the homologous Ti_nO_{2n-1}.

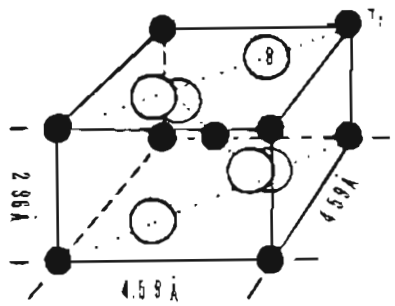

Fig.2. Rutile crystal lattice

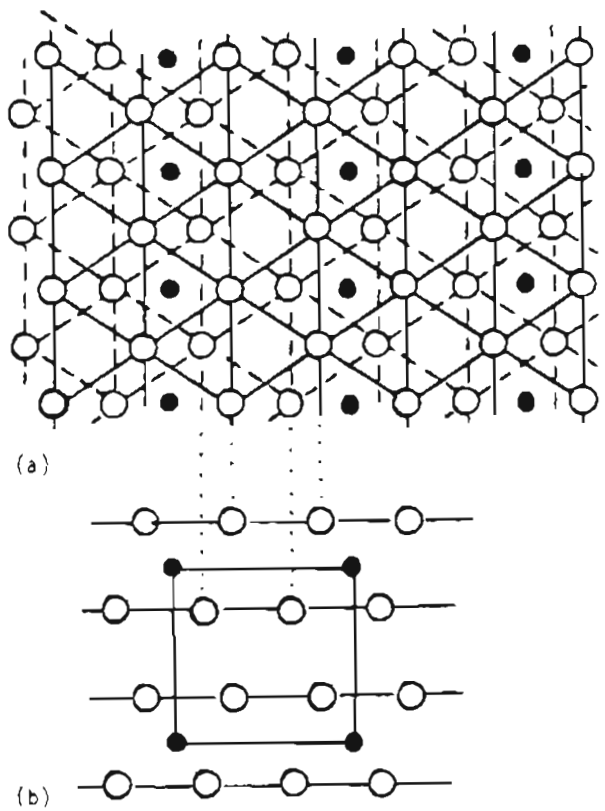

Fig.3. Projection of atom arrangement in idealized structure of rutile. Projection along b axis(a), and c axis(b).

Most of the experimental results by electrical conductivity and thermogravimetric measurement have been interpreted based on the point defect model. But the structure study in the electron microscopy by Bursill and Hyde(27) has shown that even for very small departures from stoichiometry the planar(132) planes were observed. The nominal composition of the reduced sample at 1270°K was $TiO_{1.9986}$. This corresponds to the equilibration at $P_{O_2}=10^{-15}$ atm which has been interpreted as within the point defect region. The extent of the point defect range is not clear at this point. With the increase of the concentration of point defects, the interaction between them produces extended defect aggregation. As a result many transition metal oxides develop CS planes in the reduction process.(26)

The model of generation of CS planes is described by Bursill and Hyde.(27) The schemetic illustration of the generation of defect planes is presented in Fig.4, depicting a hypothetical structure containing corner-shared MO_6 octahedra. By reduction, the oxygen vacancies created are aligned as in Fig.4a. For the next step, the lower half of the crystal is sheared in the direction marked relative to the top half of the crystal. This results in the elimination of oxygen vacancies and restoration of the coherence of the oxygen lattice as in Fig.4b.

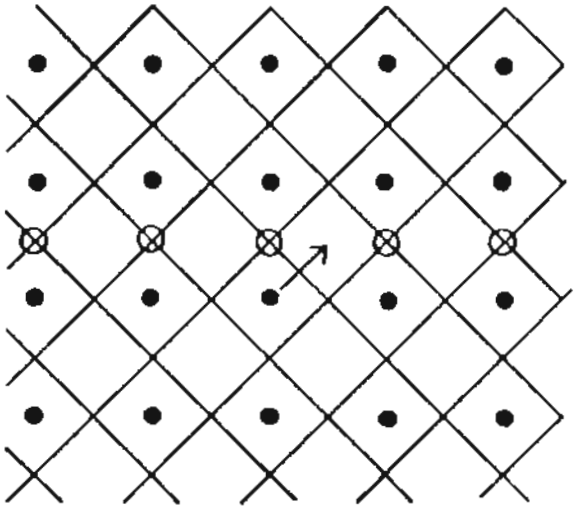

(a). Aligned vacancies(X) in cross section of hypothetical structure.

Intersection point of mesh-oxygen atom, ●metal atom. Shear direction is indicated with arrow.

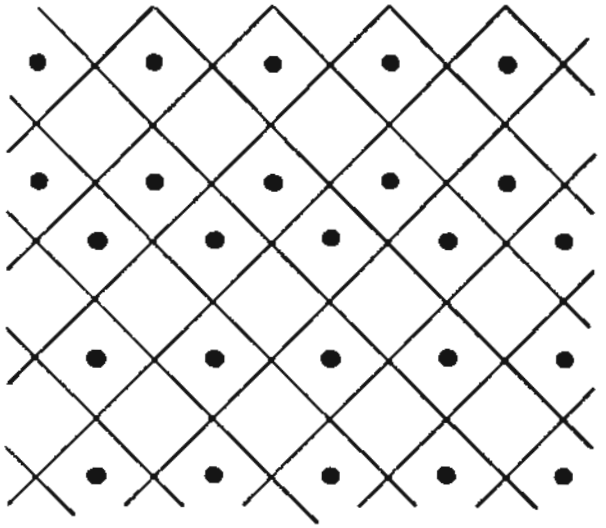

(b). After shear, oxygen sites are recovered as original with vacancy elimination.

Fig.4. Schematic diagram of generation of crystallographic shear plane(CS plane)

But the metal sub-lattice is changed at the restoration boundary. The corner sharing between MO_6 octahedra is replaced by edge-sharing. In real systems, shear plane structures are more complex. However,shear plane formation eliminates point defects by a change in the mode of linking of the MO_6 octahedra.

Basically the final state of this procedure should thermodynamically lead to a more stable state than a random distribution of point defects in the crystal. The theoretical model calculation by Catlow and James showed that the relaxation of cations at the fault plane stabilizes the extended defects.(44) By edge-sharing of MO_6 octahedra, the coordination number of the cation remains the same but that of the anions increases and the net composition results in a metal excess. The shear vector to eliminate oxygen vacancies is called the displacement vector which should be non-parallel to the defect plane to produce a non-conservative anti-phase boundary (APB).(28) The displacement vector in undoped rutile is $1/2[0\bar{1}1]_r$ lying in (100).(27) In the case of the elimination of metal interstitials point defect, the results are similar. Fig.4b shows that the regions both above and below the defect plane are the same as the original structure except for the anti-phase of metal atoms when crossing the fault

plane. When this fault planes exist in regular patterns with the same orientation, a supperlattice structure can be generated in the crystal. This is the arrangement of the atomic planes in the homologous series structure. The homologous series structure, Ti_nO_{2n-1}, was discovered as three groups, one with $4<n<9$ and (121) CS planes,(29,30) another with $16<n<36$ and (132) CS planes,(31,32) and an intermediate range where the CS planes rotate continuously from (132) to (121).(32)

For the generation of CS planes, the first step is the formation of an initial point defect aggregate. Therefore, there is an equilibrium where a certain ratio of CS planes and point defect is stabilized. Beyond the region of dominant point defects, there is a region of CS planes as dominant defect.

The isolated fault planes beyond the point defect region is mainly considered in this work. This structure is quite possible thermodynamically when we consider high concentration of point defects are developed into extended defects such as randomly spaced isolated faults.

3. THEORY

The concentrations of defects are not independent but related to each other. The nature of the interrelations among defects is studied through statistical thermodynamics.

3-1. Point defects in pure rutile.

Above the temperature of absolute zero defects are thermodynamically favorable. For pure compounds, possible defects include electronic, Frenkel, and Schottky-Wagner disorder. Electronic disorder and concentrations are described by the equiliblium equation

$$\emptyset \rightleftharpoons e' + h^{\cdot} \qquad Ki = [n][p] \text{------(1)}$$

Kröger-Vink notation is used and no interaction between defects is assumed.
Schottky-Wagner disorders and their ionized species are described as

$$\emptyset \rightleftharpoons V_{Ti} + 2V_o \qquad K_s = [V_{Ti}][V_o]^2 \text{--(2)}$$

$$V_{Ti} \rightleftharpoons V_{Ti}^{\alpha'} + \alpha h^{\cdot} \qquad K_V = \frac{[V_{Ti}^{\alpha'}][p]^{\alpha}}{[V_{Ti}]} \text{ ------(3)}$$

$$V_o \rightleftharpoons V_o^{\cdot} + e' \qquad K_1 \simeq \frac{[V_o^{\cdot}][n]}{[V_o]} \qquad \text{------(4)}$$

$$V_o^{\cdot} \rightleftharpoons V_o^{\cdot\cdot} + e' \qquad K_2 \simeq \frac{[V_o^{\cdot\cdot}][n]}{[V_o^{\cdot}]} \qquad \text{------(5)}$$

In equation(2), the cation/anion site ratio must be consistant with that of TiO_2. The lattice defects are controlled by oxygen partial pressure at equilibrium through the reaction

$$O_o \rightleftharpoons V_o + 1/2\ O_2\ (g) \quad K_o \simeq [V_o]P_{O_2}^{1/2} \text{----(6)}$$

For Frenkel disorder, the reaction is

$$Ti_{Ti} \rightleftharpoons Ti_I + V_{Ti} \quad K_F \simeq [Ti_I][V_{Ti}] \text{-----(7)}$$

$$Ti_I \rightleftharpoons Ti_I^{\alpha\cdot} + \alpha e' \qquad K_I \simeq \frac{[Ti_I^{\alpha\cdot}][n]^{\alpha}}{[Ti_I]} \qquad \text{-----(8)}$$

The titanium interstitial is related to the oxygen pressure by the reaction

$$TiO_2 \rightleftharpoons Ti_I + O_2(g) \qquad K_4 \simeq [Ti_I]P_{O_2} \quad ----(9)$$

By reduction metal excess is achieved in two ways, i.e.

$$TiO_2 \longrightarrow Ti_{Ti} + 2V_o^{\cdot\cdot} + O_2(g) \quad -----(10)$$

or

$$TiO_2 \longrightarrow Ti_I + O_2(g) \quad ------(11)$$

There can be several ionized states of titanium interstitials and vacancies. For oxygen vacancies singly and doubly ionized states are counted according to equations (4) and (5). Their relative concentrations at equilibrium depend on the position of the Fermi energy which depends on the partial pressure of oxygen.

For electrical neutrality, all positive charges are compensated by the sum of the negative charges,

$$[n] + \alpha[V_{Ti}^{\alpha'}] = [p] + [V_o^{\cdot}] + 2[V_o^{\cdot\cdot}] + \beta[Ti_I^{\beta\cdot}] \quad ----(12)$$
$$(1 < \alpha, \beta < 4)$$

If the Schottky-Wagner type of disorder is more favorable in the vicinity of stoichiometry($K_s > K_F, K_i$), tetravalent

metal vacancies and divalent oxygen vacancies are predominant for the neutrality condition of equation (12) and are approximately constant in concentration. All other defects are negligible because of relatively small concentration. Therefore equation (12) is approximated as

$$4[V_{Ti}^{4'}] \simeq 2[V_O^{\cdot\cdot}] = \text{Const.}$$

With this limiting condition, the results of the pressure dependence of the other defects are listed in Table 1. Decreasing P_{O_2} increases positively charged atomic defects which are compensated electronically. This corresponds to the shift of the Fermi level toward the conduction band. Meanwhile, the concentration of metal vacancies decrease. The neutrality condition for the next decreasing P_{O_2} region is approximated as

$$[n] \simeq 2[V_O^{\cdot\cdot}]$$

For lower oxygen partial pressure, the Fermi level becomes closer to the conduction band which leads to a higher probability of electron occupation on oxygen vacancies as well as an increase in vacancy concentration. This leads to new approximation of the neutrality condition,

	$[n] = [V_O^{\cdot\cdot}]$	$[n] = 2[V_O^{\cdot\cdot}]$	$4[V_{Ti}^{4\prime}] = 2[V_O^{\cdot\cdot}]$	$4[V_{Ti}^{4\prime}] = [p]$
n	$(K_O K_1)^{1/2} P_{O_2}^{-1/4}$	$(2K_O K_1 K_2)^{1/3} P_{O_2}^{-1/6}$	$\left(\frac{K_O^3 K_i^4 K_1 K_2}{2K_s K_v}\right)^{1/6} P_{O_2}^{-1/4}$	$\left(\frac{K_i^5 K_O^2}{4K_s K_v}\right)^{1/5} P_{O_2}^{-1/5}$
p	$\left(\frac{K_i^2}{K_O K_1}\right)^{1/2} P_{O_2}^{1/4}$	$\left(\frac{K_i^3}{2K_O K_1 K_2}\right)^{1/3} P_{O_2}^{1/6}$	$\left(\frac{2K_s K_v K_i^2}{K_O^3 K_1 K_2}\right)^{1/6} P_{O_2}^{1/4}$	$\left(\frac{4K_s K_v}{K_O^2}\right)^{1/5} P_{O_2}^{1/5}$
$V_O^{\cdot\cdot}$	$(K_O K_1)^{1/2} P_{O_2}^{-1/4}$	$\left(\frac{K_O^2 K_1^2}{2K_2}\right)^{1/3} P_{O_2}^{-1/3}$	$\left(\frac{2K_s K_v K_O^3 K_1^5}{K_i^4 K_2}\right)^{1/6} P_{O_2}^{-1/4}$	$\left(\frac{4K_O^3 K_1^5 K_s K_v}{K_i^5}\right)^{1/5} P_{O_2}^{-3/10}$
$V_O^{\prime\prime}$	K_2	$\left(\frac{K_O K_1 K_2}{4}\right)^{1/3} P_{O_2}^{-1/6}$	$\left(\frac{2K_s K_v K_1^2 K_2^2}{K_i^4}\right)^{1/3}$	$\frac{K_1 K_2}{K_i^2}(16 K_O K_s K_v)^{1/5} P_{O_2}^{-1/10}$
$V_{Ti}^{4\prime}$	$\frac{K_s K_v K_1^2}{K_i^4}$	$\frac{K_s K_v}{}\left(\frac{4K_1^2 K_2^2}{K_O}\right)^{2/3} P_{O_2}^{1/3}$	$\left(\frac{K_s K_v K_1^2 K_2^2}{4K_i^4}\right)^{1/3}$	$\frac{1}{4}\left(\frac{4K_s K_v}{K_O^2}\right)^{1/5} P_{O_2}^{1/5}$
V_O	$K_O P_{O_2}^{-1/2}$	$K_O P_{O_2}^{-1/2}$	$K_O P_{O_2}^{-1/2}$	$K_O P_{O_2}^{-1/2}$
V_{Ti}	$\frac{K_s}{K_O^2} P_{O_2}$	$\frac{K_s}{K_O^2} P_{O_2}$	$\frac{K_s}{K_O^2} P_{O_2}$	$\frac{K_s}{K_O^2} P_{O_2}$

Table 1. Pressure dependence of defect concentration in pure rutile for $K_s > K_i, K_F$

$$[n] \simeq [V_O^{\cdot}]$$

The concentration profile of defect species with corresponding neutrality condition is shown in Fig.5.

When Frenkel defects are dominant near stoichiometry, the prevailing defects for each neutrality condition are different. The concentration profiles for this case is given in Table 2 and Fig.6.

For the last case, electronic disorder may prevail over lattice defects near stoichiometry. These conditions are presented in Table 3,4, and Fig.7 and 8.

The electrical conductivity is related to the concentration of charge carrier as

$$\sigma = \sum \mu_i (Z_i q_i)[Ci] \qquad \text{------(13)}$$

where Ci is carrier concentration, μ_i mobility and Zi valency of carrier i.

The mobility of the charge carrier is a function of temperature. Ionic mobilty is several orders less than that of electrons and electron holes. Therefore, electrical conductivity generally depends on the concentrations of electrons and electron holes except where ionic conductivity is dominant. The concentration of charge carriers

	$[n] = 4[Ti_I^{4\cdot}]$	$4[V_{Ti}^{4\prime}] = 4[Ti_I^{4\cdot}]$	$4[V_{Ti}^{4\prime}] = [p]$
n	$(4K_IK_4)^{1/5}P_{O_2}^{-1/5}$	$(\frac{K_I}{K_v})^{1/8}K_i^{1/2}K_4^{1/4}P_{O_2}^{-1/4}$	$K_i(\frac{K_4}{4K_vK_F})^{1/5}P_{O_2}^{-1/5}$
p	$\frac{K_i}{(4K_IK_4)^{1/5}}P_{O_2}^{1/5}$	$(\frac{K_i^4}{K_4K_I})^{1/8}P_{O_2}^{1/4}$	$(\frac{4K_vK_F}{K_4})^{1/5}P_{O_2}^{1/5}$
$Ti_I^{4\cdot}$	$\frac{1}{4}(4K_IK_4)^{1/5}P_{O_2}^{-1/5}$	$\frac{(K_FK_IK_V)^{1/2}}{K_i^2}$	$\frac{K_I}{K_i^4}(4K_VK_F)^{4/5}K_4^{1/5}P_{O_2}^{-1/5}$
$V_{Ti}^{4\prime}$	$\frac{K_vK_F}{K_i^4K_4^{1/4}}(4K_I)^{4/5}P_{O_2}^{1/5}$	$\frac{(K_FK_IK_v)^{1/2}}{K_i^2}$	$\frac{1}{4}(\frac{4K_vK_F}{K_4})^{1/5}P_{O_2}^{1/5}$
Ti_I	$K_4P_{O_2}^{-1}$	$K_4P_{O_2}^{-1}$	$K_4P_{O_2}^{-1}$
V_{Ti}	$\frac{K_F}{K_4}P_{O_2}$	$\frac{K_F}{K_4}P_{O_2}$	$\frac{K_F}{K_4}P_{O_2}$

Table 2. Pressure dependence of defect concentration in pure rutile for $K_F > K_i, K_s$.

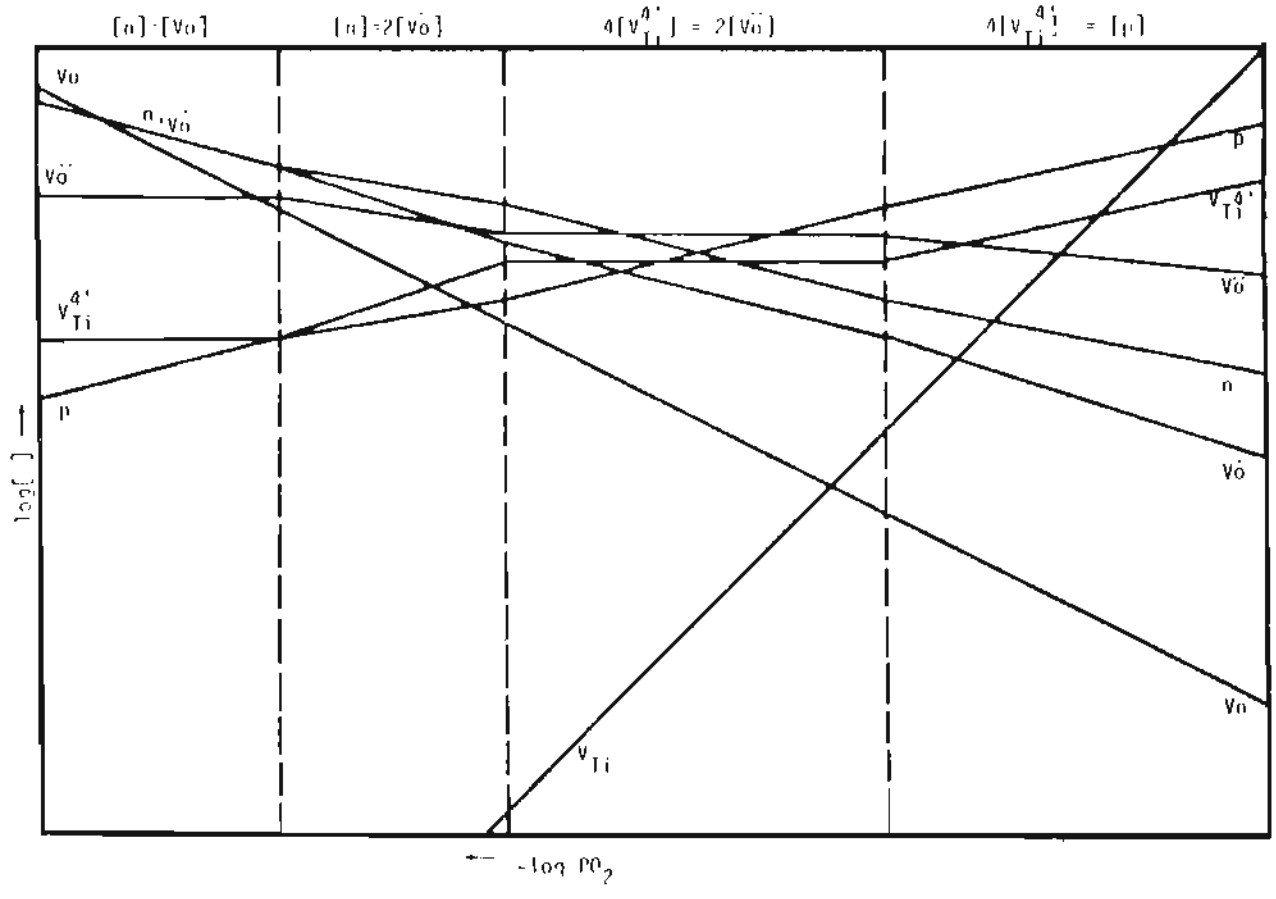

Fig.5. Concentration profile of defects of pure rutile for $K_S > K_i, K_F$.

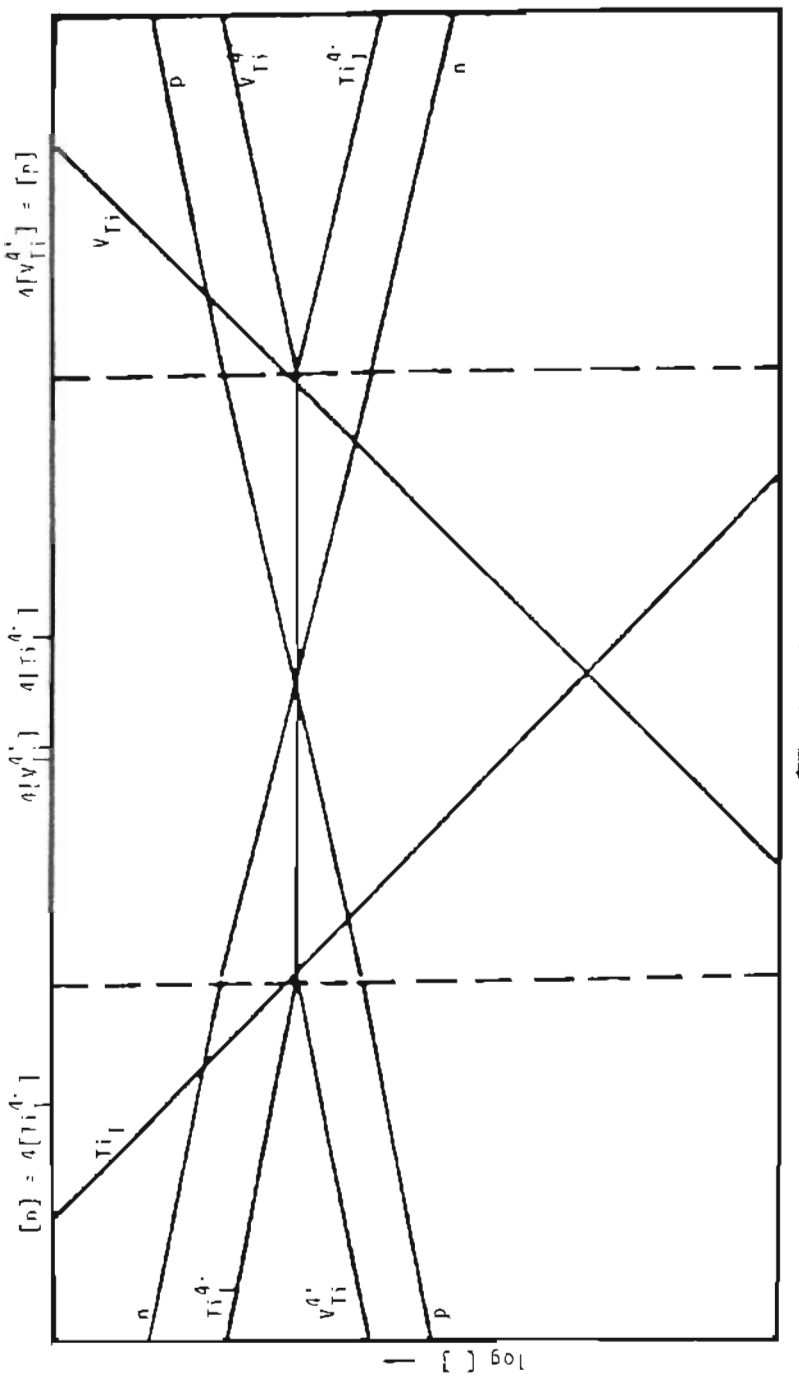

Fig.6. Concentration profile of defects of pure rutile for $K_F > K_i$, K_s.

	$[n] = [V_O^{\cdot}]$	$[n] = 2[V_O^{\cdot}]$	$[n] = [p]$	$4[V_{Ti}^{4'}] = [p]$
n	$(K_O K_1)^{1/2} P_{O_2}^{-1/4}$	$(2K_O K_1 K_2)^{1/3} P_{O_2}^{-1/6}$	$K_i^{1/2}$	$K_i \left(\frac{K_O^2}{4K_s K_v}\right)^{1/5} P_{O_2}^{-1/5}$
p	$\left(\frac{K_i^2}{K_O K_1}\right)^{1/2} P_{O_2}^{1/4}$	$\frac{K_i}{(2K_O K_1 K_2)^{1/3}} P_{O_2}^{1/6}$	$K_i^{1/2}$	$\left(\frac{4K_s K_v}{K_O^2}\right)^{1/5} P_{O_2}^{1/5}$
$V_O^{\cdot}$	$(K_O K_1)^{1/2} P_{O_2}^{-1/4}$	$\left(\frac{K_1^2 K_O^2}{2K_2}\right)^{1/3} P_{O_2}^{-1/3}$	$\frac{K_O K_1}{(K_i)^{1/2}} P_{O_2}^{-1/2}$	$\left(\frac{4K_O^3 K_1^5 K_s K_v}{K_i^5}\right)^{1/5} P_{O_2}^{-3/10}$
$V_O^{\cdot}$	K_2	$\left(\frac{K_O K_1 K_2}{4}\right)^{1/3} P_{O_2}^{-1/6}$	$\left(\frac{K_O K_1 K_2}{K_i}\right) P_{O_2}^{-1/2}$	$\frac{K_1 K_2}{K_i^2}\left(16 K_O K_s^2 K_v^2\right)^{1/5} P_{O_2}^{-1/10}$
$V_{Ti}^{4'}$	$\frac{K_s K_v K_i^2}{K_i^4}$	$\frac{K_s K_v}{K_i^4}\left(\frac{4K_i^2 K_2^2}{K_O}\right)^{2/3} P_{O_2}^{1/3}$	$\left(\frac{K_s K_v}{K_O^2 K_1^2}\right) P_{O_2}$	$\frac{1}{4}\left(\frac{4K_s K_v}{K_O^2}\right)^{1/5} P_{O_2}^{1/5}$
V_O	$K_O P_{O_2}^{-1/2}$	$K_O P_{O_2}^{-1/2}$	$K_O P_{O_2}^{-1/2}$	$K_O P_{O_2}^{-1/2}$
V_{Ti}	$\frac{K_s}{K_O^2} P_{O_2}$	$\frac{K_s}{K_O^2} P_{O_2}$	$\frac{K_s}{K_O^2} P_{O_2}$	$\frac{K_s}{K_O^2} P_{O_2}$

Table 3. Pressure dependence of defect concentration in pure rutile for $K_i > K_s$.

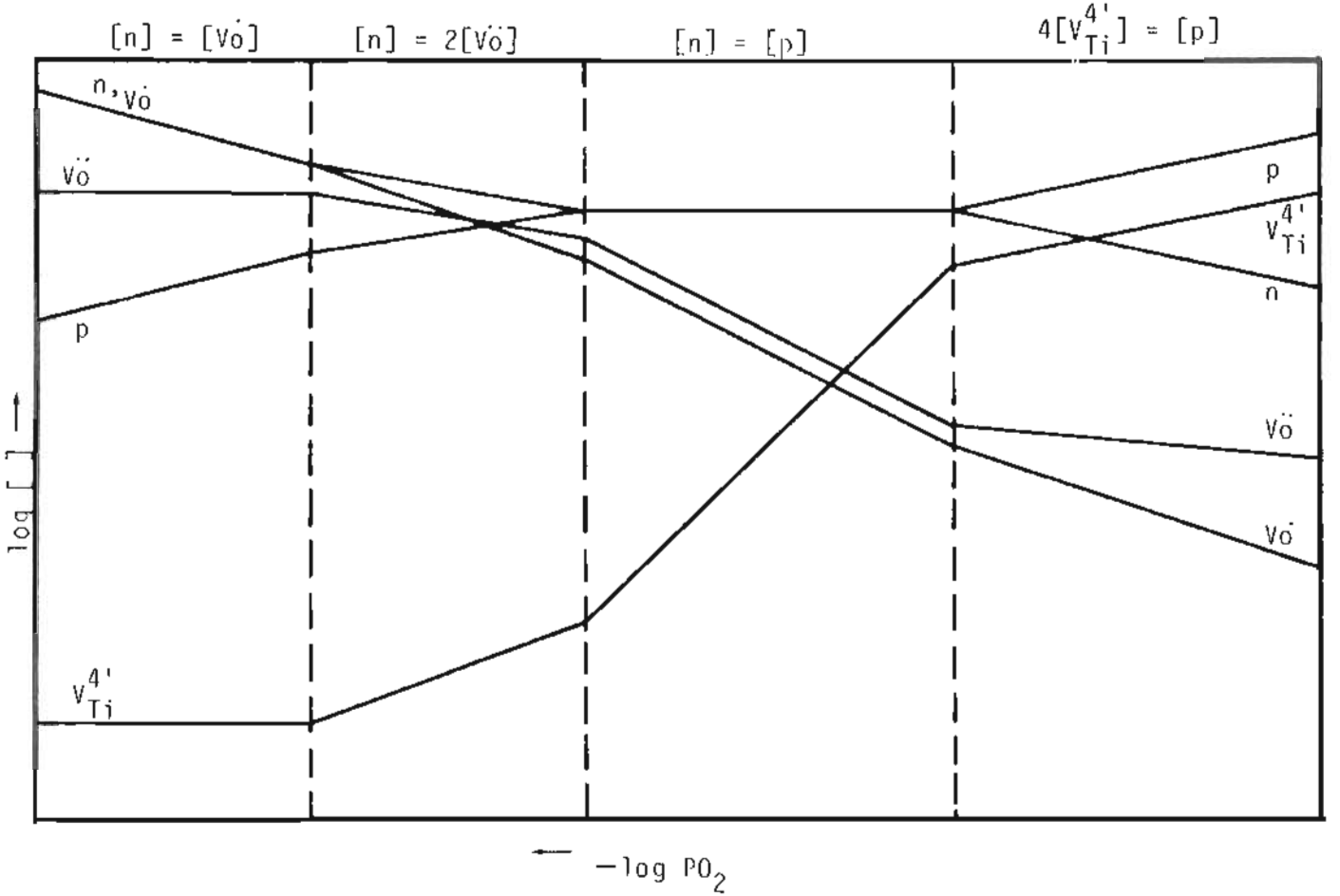

Fig.7. Concentration profile of defects of pure rutile for $K_i > K_s$

	$[n] = 4[Ti_I^{4\cdot}]$	$[n] = [p]$	$4[V_{Ti}^{4'}] = [p]$
n	$(4K_IK_4)^{1/5}P_{O_2}^{-1/5}$	$K_i^{1/2}$	$K_i(\frac{K_4}{4K_vK_F})^{1/5}P_{O_2}^{-1/5}$
p	$\frac{K_i}{(4K_IK_4)^{1/5}}P_{O_2}^{1/5}$	$K_i^{1/2}$	$(\frac{4K_vK_F}{K_4})^{1/5}P_{O_2}^{1/5}$
$Ti_I^{4\cdot}$	$\frac{1}{4}(4K_IK_4)^{1/5}P_{O_2}$	$\frac{K_IK_4}{K_i^2}P_{O_2}^{-1}$	$\frac{K_I}{K_i^4}(4K_vK_F)^{4/5}(K_4)^{1/5}P_{O_2}^{-1/5}$
$V_{Ti}^{4'}$	$\frac{K_vK_F}{K_i^4K_4^{1/4}}(4K_2)^{4/5}P_{O_2}^{1/5}$	$\frac{K_vK_F}{K_i^2K_4}P_{O_2}$	$\frac{1}{4}(\frac{4K_vK_F}{K_4})^{1/5}P_{O_2}^{1/5}$
Ti_I	$K_4P_{O_2}^{-1}$	$K_4P_{O_2}^{-1}$	$K_4P_{O_2}^{-1}$
V_{Ti}	$\frac{K_F}{K_4}P_{O_2}$	$\frac{K_F}{K_4}P_{O_2}$	$\frac{K_F}{K_4}P_{O_2}$

Table 4. Pressure dependence of defect concentration in pure rutile for $K_i > K_F$.

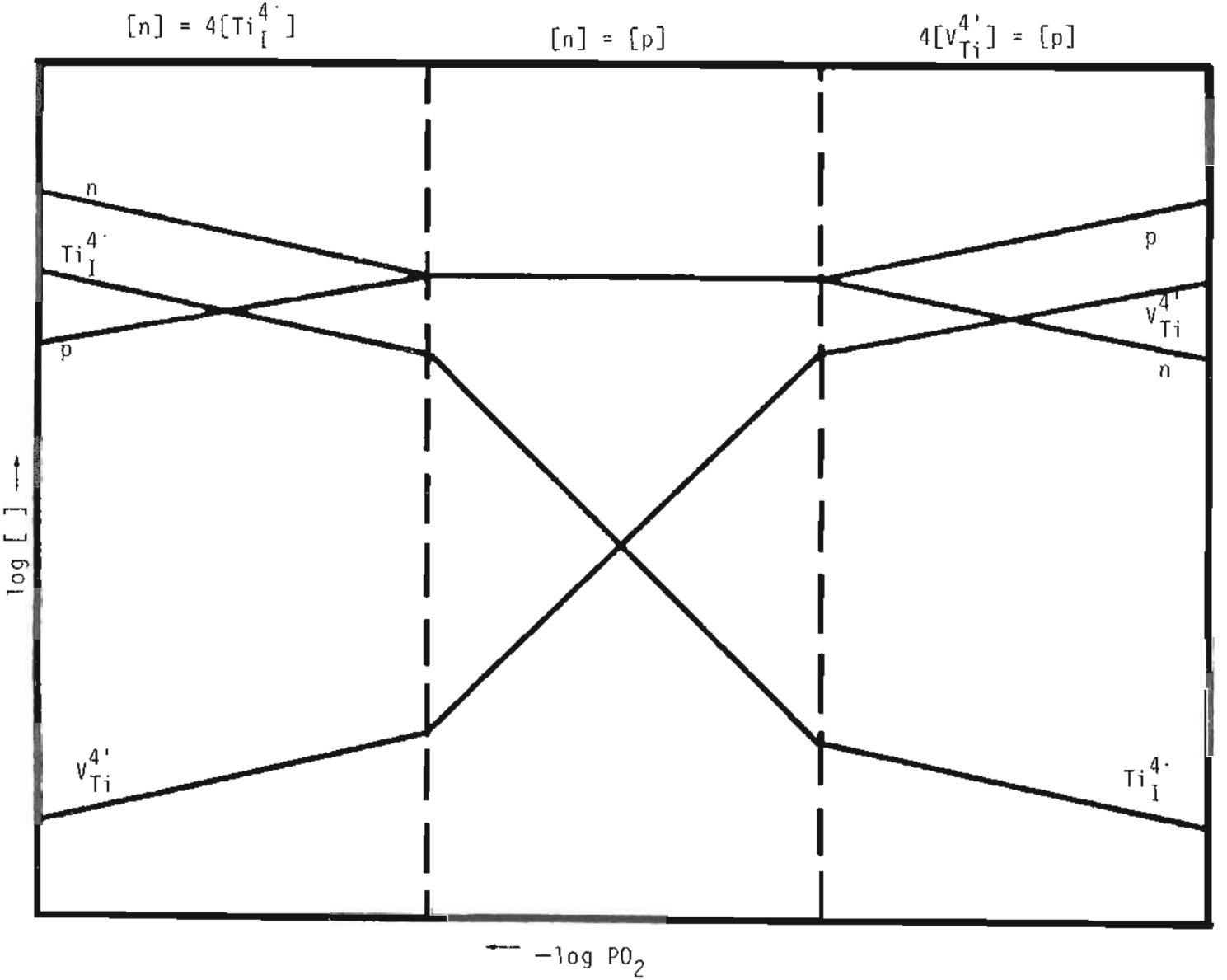

Fig.8. Concentration profile of defects of pure rutile for $K_i > K_F$

depends on oxygen partial pressure in a particular way for a given neutrality condition. From this dependence, the type of the main charge carrier can be determined by conductivity measurements.

3-2. Defects in a crystal containing foreign atoms.

All crystals contain foreign atoms as impurities. The site of occupation of foreign atoms depends on factors such as size, valency, and electronegativity. Foreign atoms tend to occupy the position of ions to which it is closest on the electronegativity scale. If the difference in electronegativity is small, size factor dominates the consideration of occupation site. Small foreign atoms can also occupy interstitial sites. Addition of ions on interstitial sites or substitutional occupation by ions of different valency requires associated charge balance to maintain electrical neutrality of the crystal. This can be accomplished by vacancy formation or changes in electronic disorder.

Let us consider acceptor doping, M_2O_3 incorporation with Schottky-Wagner defects. Assuming substitutional occupation of M^{3+}

$$M_2O_3 \xrightarrow{TiO_2} 2M_{Ti}' + 3O_O + V_O^{\cdot\cdot} \qquad \text{-------(14)}$$

at low oxygen partial pressure and

$$M_2O_3 + 1/2\ O_2 \xrightarrow{TiO_2} 2M'_{Ti} + 2\dot{h} + 4O_O \qquad \text{------(15)}$$

at high oxygen partial pressure.

The total doping level is fixed and the concentrations of neutral and ionized dopant are related ;

$$M_{Ti} \rightleftharpoons M'_{Ti} + \dot{h} \qquad K_5 \simeq \frac{[M'_{Ti}][p]}{[M_{Ti}]} \qquad \text{------(16)}$$

$$[M_{Ti}]_{total} = [M_{Ti}] + [M'_{Ti}] \simeq \text{Const.} \qquad \text{------(17)}$$

The electrical neutrality condition becomes

$$[n] + 4[V_{Ti}^{4'}] + [M'_{Ti}] = [p] + [V_O^{\cdot}] + 2[V_O^{\cdot\cdot}] \qquad \text{------(18)}$$

At extreme regions of both low and high partial pressure, the intrinsic disorders prevail and the Fermi level is close to the conduction and valence bands respectively. For intermediate regions of pressure, the approximate electrical neutrality conditions and concentration profiles are given in Table 5. and Fig.9. We should bear in mind

	$[n] = [V_O^{\cdot}]$	$[n] = 2[V_O^{\cdot\cdot}]$	$2[V_O^{\cdot\cdot}] = [M_{Ti}']$		$[M_{Ti}'] = [p]$	$4[V_{Ti}^{4'}] = [p]$
			$[M_{Ti}'] = [M_{Ti}']_T$	$[M_{Ti}] = [M_{Ti}]_T$		
n	-1/4	-1/6	-1/4	-1/6	0	-1/5
p	1/4	1/6	1/4	1/6	0	1/5
$V_O^{\cdot}$	-1/4	-1/3	-1/4	-1/3	-1/2	-3/10
$V_O^{\cdot\cdot}$	0	-1/6	0	-1/6	-1/2	-1/10
M_{Ti}'	0	0	0	-1/6	0	-1/5
$V_{Ti}^{4'}$	0	1/3	0	1/3	1	1/5
M_{Ti}	1/4	1/6	1/4	0	0	0
V_{Ti}	1	1	1	1	1	1
V_O	-1/2	-1/2	-1/2	-1/2	-1/2	-1/2

Table 5. Pressure dependence of defect concentration in acceptor-doped rutile with Schottky-Wagner disorder(m values of $P_{O_2}^{-m}$ dependence).

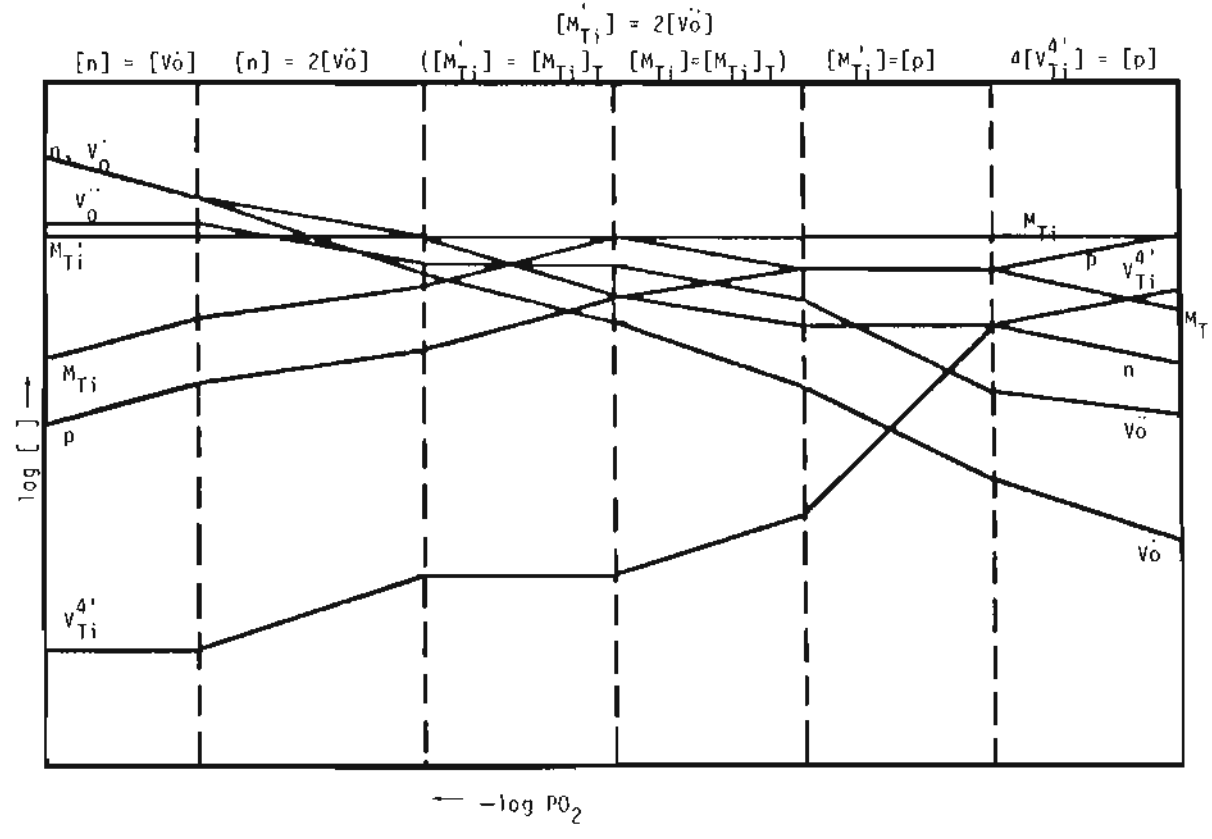

Fig.9. Concentration profile of defects of acceptor-doped rutile with Schottky-Wagner disorder.

that all regions are possible but in practical experiments some ranges are too narrow to be observed or may not even occur.

At high oxygen partial pressure, acceptors produce electron holes when they occupy lattice sites as in equation (15). As a result, the n-p transition region is shifted to lower oxygen partial pressures with increasing acceptor dopant concentration.

For acceptor dopants associated with Frenkel disorder, the reaction at low P_{O_2} is

$$2M_2O_3 + Ti_{Ti} \xrightarrow{TiO_2} 4M'_{Ti} + Ti_I^{4\cdot} + 6O_O \quad \text{------(19)}$$

The total electrical neutrality condition is

$$[n] + 4[V_{Ti}^{4'}] + [M'_{Ti}] = [p] + 4[Ti_I^{4\cdot}] \quad \text{------(20)}$$

At high oxygen partial pressures, acceptors are compensated electronically according to quation (15). The concentration profile and its dependence on oxygen partial pressure with proper neutrality conditions are in Table 6 and Fig.10.

When higher valence foreign atoms (donor, M_2O_5) are added substitutionally into rutile, the energy center

	$[n] = 4[Ti_I^{4\cdot}]$	$[M'_{Ti}] = 4[Ti_I^{4\cdot}]$		$[M'_{Ti}] = [p]$	$4[V_{Ti}^{4'}] = [p]$
		$[M'_{Ti}] = [M_{Ti}]_T$	$[M_{Ti}] = [M_{Ti}]_T$		
n	-1/5	-1/4	-1/5	0	-1/5
p	1/5	1/4	1/5	0	1/5
$Ti_I^{4\cdot}$	-1/5	0	-1/5	-1	-1/5
$V_{Ti}^{4'}$	1/5	0	1/5	1	1/5
M'_{Ti}	0	0	-1/5	0	-1/5
M_{Ti}	1/5	1/4	0	0	0
Ti_I	-1	-1	-1	-1	-1
V_{Ti}	1	1	1	1	1

Table 6. Pressure dependence of defect concentration in acceptor-doped rutile associated with Frenkel disorder(m values of $P_{O_2}^{-m}$ dependence).

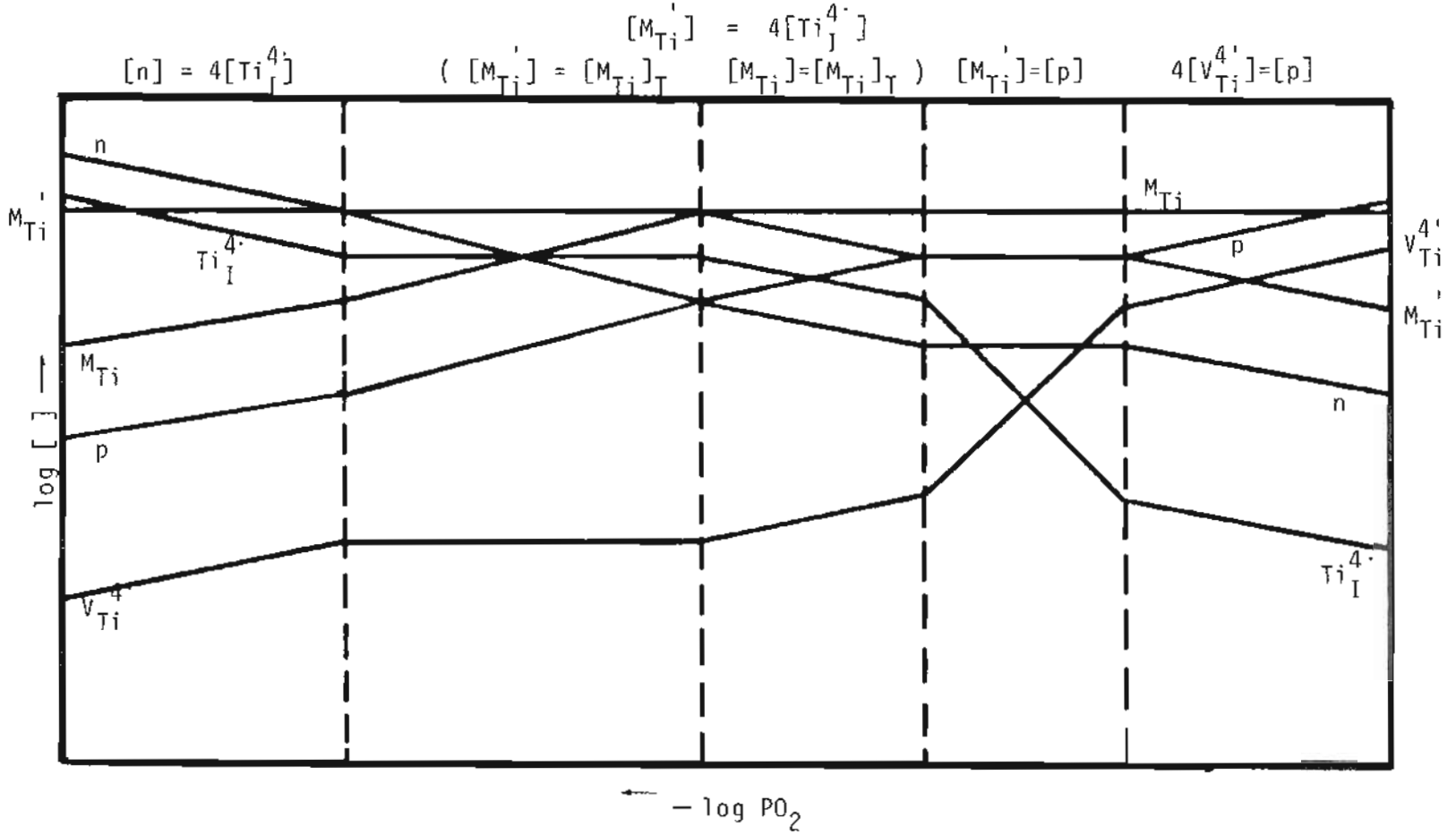

Fig.10. Concentration profile of acceptor-doped rutile with Frenkel disorder.

of this defect is close to the conduction band. For Schottky-Wager disorder compensating the donor at high oxygen partial pressure, the reaction is as

$$2M_2O_5 \xrightarrow{TiO_2} 4M_{Ti} + V_{Ti} + 10\ O_o \quad \text{------(21)}$$

At low oxygen partial pressure

$$M_2O_5 \xrightarrow{TiO_2} 2M_{Ti} + 2e' + 4O_o + 1/2\ O_2(g) \quad \text{----(22)}$$

The neutrality condition is

$$[n] + 4[V_{Ti}^{4'}] = [p] + [M_{Ti}^{\cdot}] + [V_o^{\cdot}] + 2[V_o^{\cdot\cdot}] \quad \text{----(23)}$$

For donor ionization

$$M_{Ti} \rightleftharpoons M_{Ti}^{\cdot} + e' \qquad K_6 \simeq \frac{[M_{Ti}^{\cdot}][n]}{[M_{Ti}]} \quad \text{------(24)}$$

$$[M_{Ti}] + [M_{Ti}^{\cdot}] = [M_{Ti}]_{total} = \text{Const.} \quad \text{-----(25)}$$

If Frenkel disorder is more favorable for the donor compensation, the neutrality condition is

$$[n] + 4[V_{Ti}^{4'}] = [p] + [M_{Ti}^{\cdot}] + 4[Ti_{I}^{4\cdot}] \quad \text{----(25')}$$

The dependence of defect concentration and corresponding neutrality condition on oxygen partial pressure are given in Table 7-8, and Fig. 11-12. It is assumed that the donor center is closer to the conduction band than that of the tetravalent titanium interstitial.

We have considered many possible cases of pure and doped rutile in terms of the equilibrium defect structure. Only through experimental observation can we determine which are actually achieved.

	$[n] = [V_O^{\cdot}]$	$[n] = 2[V_O^{\cdot\cdot}]$	$[n]=[M_{Ti}^{\cdot}]=[M_{Ti}]_T$	$[M_{Ti}^{\cdot}] = 4[V_{Ti}^{4'}]$	$4[V_{Ti}^{4'}] = [p]$
n	-1/4	-1/6	0	-1/4	-1/5
p	1/4	1/6	0	1/4	1/5
$V_O^{\cdot}$	-1/4	-1/3	-1/2	-1/4	-3/10
$V_O^{\cdot\cdot}$	0	-1/6	-1/2	0	-1/10
$V_{Ti}^{4'}$	0	1/3	1	0	1/5
$M_{Ti}^{\cdot}$	1/4	1/6	0	0	0
M_{Ti}	0	0	0	-1/4	-1/5
V_O	-1/2	-1/2	-1/2	-1/2	-1/2
V_{Ti}	1	1	1	1	1

Table 7. Pressure dependence of defect concentration in donor-doped rutile with Schottky-Wagner disorder(m values of $P_{O_2}^{-m}$).

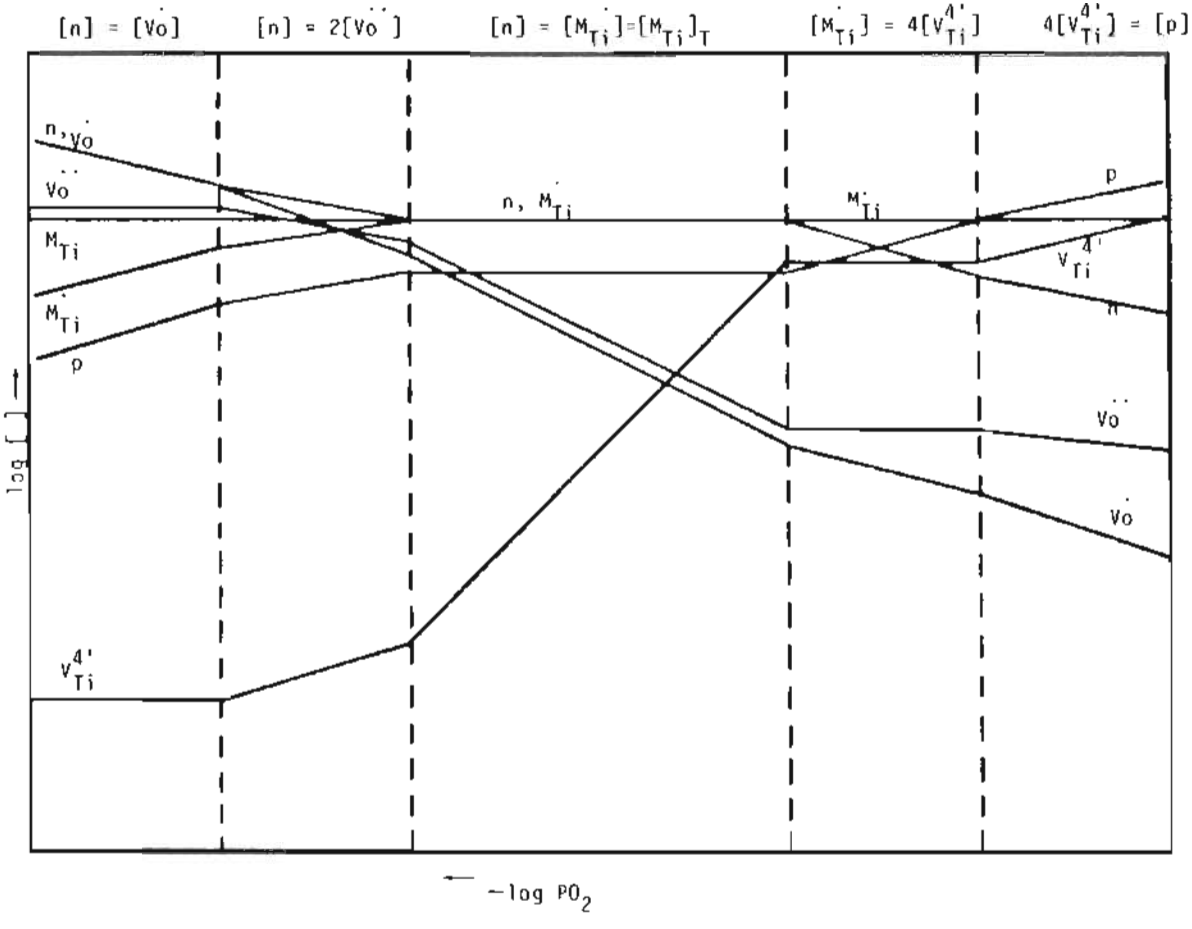

Fig.11. Concentration profile of defects of donor-doped rutile with Schottky-Wagner disorder.

	$n = 4[Ti_I^{4\cdot}]$	$[n] = [M_{Ti}^{\cdot}] = [M_{Ti}]_T$	$[M_{Ti}^{\cdot}] = 4[V_{Ti}^{4'}]$	$4[V_{Ti}^{4'}] = [p]$
n	-1/5	0	-1/4	-1/5
p	1/5	0	1/4	1/5
$Ti_I^{4\cdot}$	-1/5	-1	0	-1/5
$V_{Ti}^{4'}$	1/5	1	0	1/5
$M_{Ti}^{\cdot}$	1/4	0	0	0
M_{Ti}	0	0	-1/4	-1/5
Ti_I	-1	-1	-1	-1
V_{Ti}	1	1	1	1

Table 8. Pressure dependence of defect concentration in donor-doped rutile with Frenkel disorder(m values of $P_{O_2}^{-m}$).

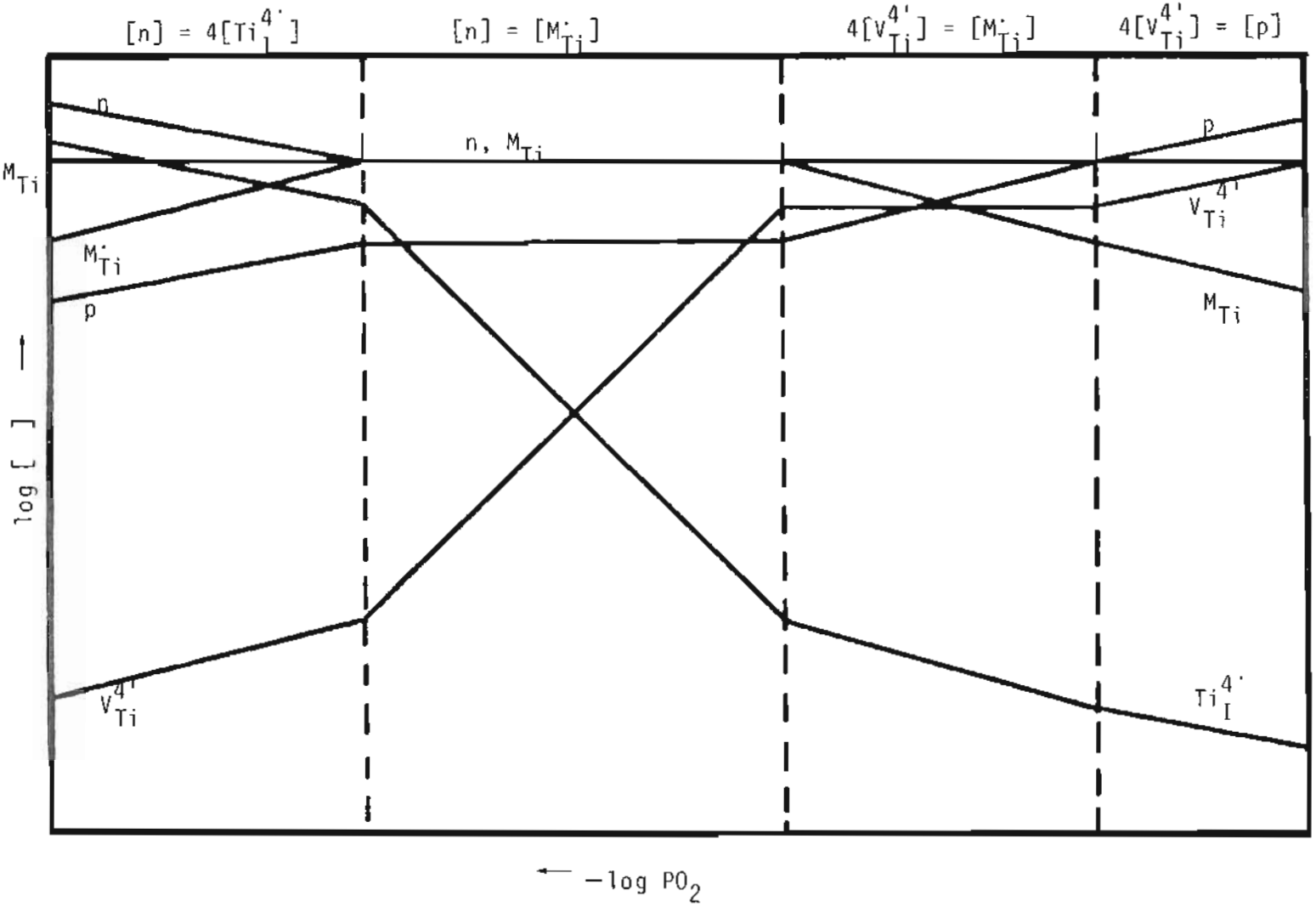

Fig.12. Concentration profile of defects of donor-doped rutile with Frenkel disorder.

4. OBJECTIVES

We have demonstrated that there are many possible types of defects developed when a material is equilibrated with a controlled oxygen activity. From the results observed by several investigators, there is disagreement on the type of equilibrium defect in a given region of nonstoichiometry. This may be attributed to extrinsic behavior caused by unknown impurities, nonhomogeneity, or experimental error such as equilibrium not being reached. For example, it takes nearly 120 hrs to reach equilibrium at 1000°C at $P_{O_2}=10^{-9}$ atm.

In order to produce homogeneous specimens, a liquid mix technique is employed for materials preparation in this experiment. Further investigation of the effect of dopants on the sudden increase in conductivity at very low oxygen activities will be conducted. An equilibrium defect model will be developed to explain this anomalous behavior that is inconsistent with traditional point defects.

The materials investigated will be undoped and doped polycrystalline rutile. Electrical conductivity measurements together with microstructure analysis by T.E.M. will be performed to determine the possibility of the coexistance of extended and point defects as a function of equilibrium oxygen activity.

5. EXPERIMENTAL PROCEDURE

5-1. Sample preparation

All samples were prepared by the "Liquid Mix Technique".(33,34) The main advantage of this technique from other chemical preparation methods or conventional mixed solid phase reaction is to obtain an amorphous precursor(polymeric glass) homogeneously retaining all the necessary metallic ions homogeneously before final oxide formation.

A precursor of the mixed oxide can be obtained from solutions containing all the required ions and organic polyfunctional acid. The final oxide solid solution is produced by pyrolysis of the precursor at 600°-700°C a relatively low temperature compared to the required solid-solid phase reaction temperatures.

The starting solution for TiO_2 was tetraisopropyl titanate solution (Dupont Co. Tizor). Tantalum oxalate solution was prepared from a known amount of tantalum oxalate (Kawecki Beryl Co. Industries, Boyer town, Penn.) dissolved in the ethylene glycol-citric acid solution. Likewise chromium nitrate was dissolved in the same organic mixed solution.

The doping concentration of the solution was analysed gravimetryically. Tetraisopropyl titanate solution and ethylene glycol-citric acid solution containing the doping cations were homogeneously mixed, then evaporated to the rigid polymeric glassy state followed by calcination at 700°C for 5 hrs. The calcined powders were pressed into pellets at 30K psi and sintered at 1350°C for 12 hrs in air.

5-2 Gas preparation.

The gases employed to adjust the controlled atmosphere were pure oxygen and analysed oxygen argon mixtures for high oxygen partial pressure, and CO/CO_2 gas mixtures for low partial pressures. All the gases were purified prior to mixing. Columns of ascarite, magnesium perchlorate and drierite were used to absorb carbon dioxide and water respectively.

The main impurities in cylinder carbon monoxide are moisture, carbon dioxide and iron carbonyl. Purification from iron carbonyl is difficult. Sometimes active iron from iron carbonyl possibly deposits on the wall of the furnace tube.

Carbon monoxide gas was passed through the columns of

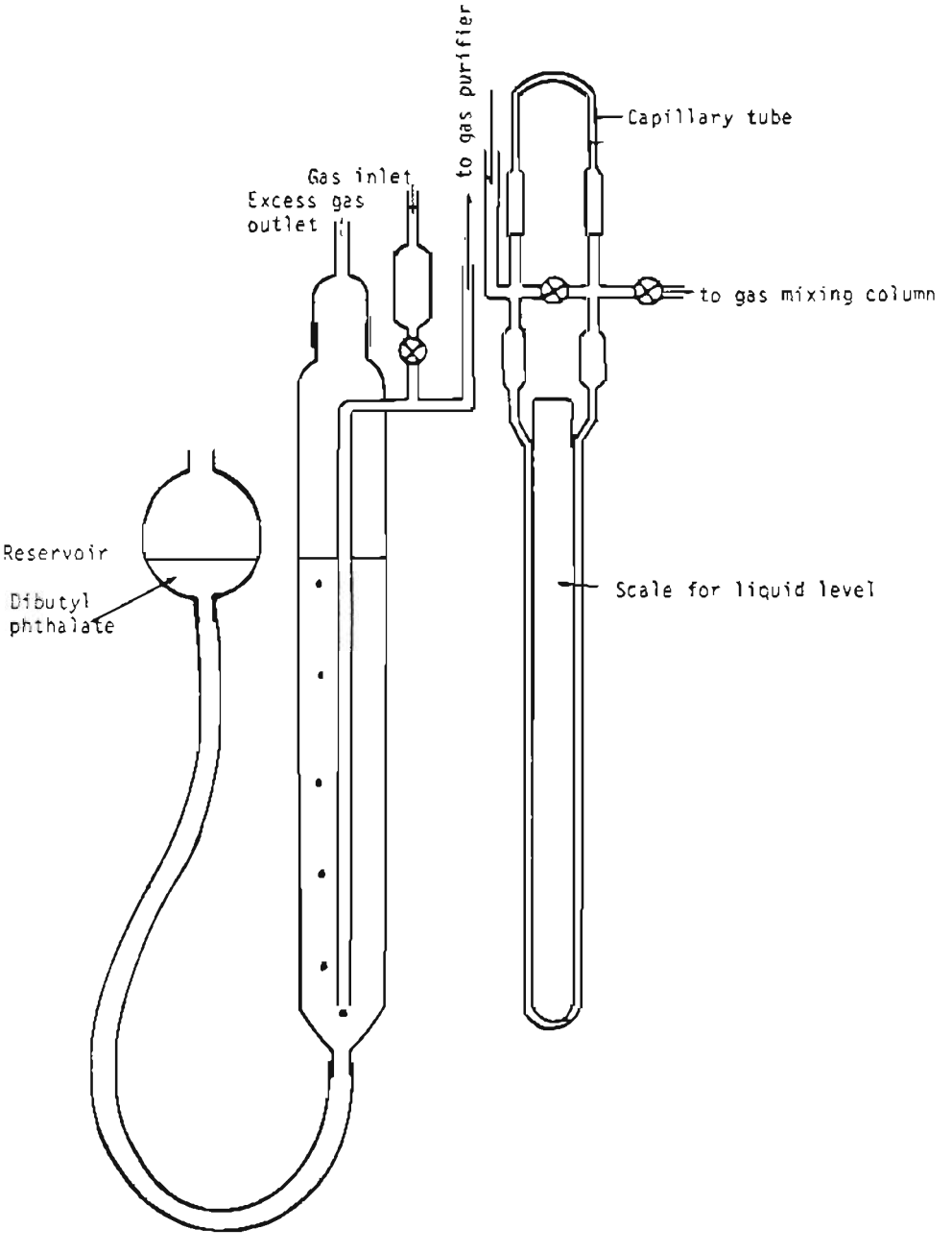

Fig.13. Diagram of a constant pressure head flowmeter.

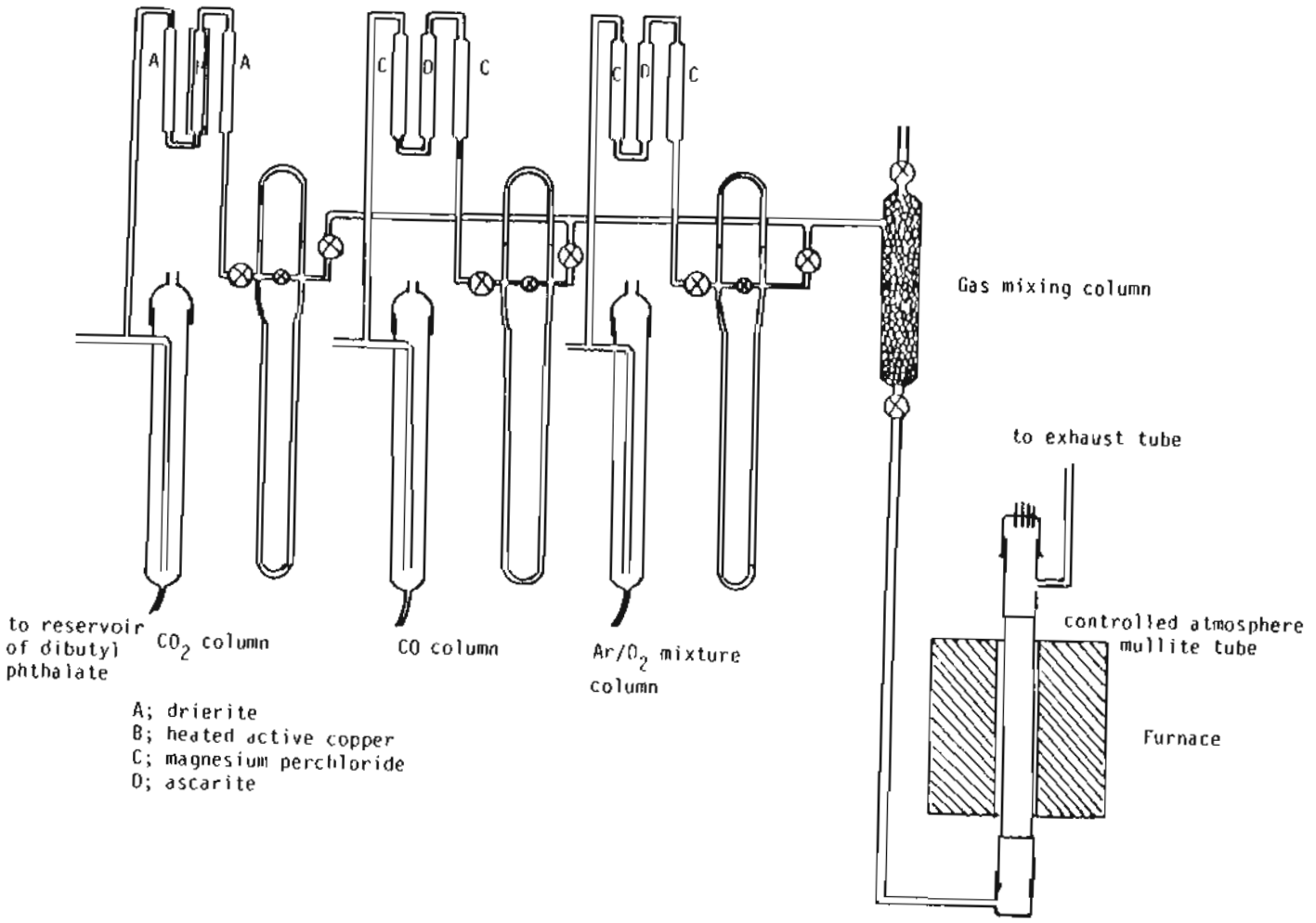

Fig.14. Schematic diagram of manometer and furnace connection.

magnesium perchlorate, ascarite, magnesium perchlorate. Carbon dioxide gas flowed through drierite, heated active copper(450°C), and drierite columns. The oxygen and oxygen-argon mixtures were passed through same sequence of columns as carbon monoxide.

Low oxygen partial pressures were established by obtaining the equilibrium state from a given gas mixture calculated from known thermodynamic data. The corresponding volume ratios of CO/CO_2 gas mixtures for a certain oxygen partial pressure at the experimental temperature can be obtained from tabulation of thermodynamic data.(35) The mixing ratios of gases were prepared by using conventional manometric flow meters. The basic principle of the meter is to maintain a constant pressure drop through the flow meter by means of fixing the level of dibutyl phthalate in the gas blow-off column by transferring the fluid from the reservoir(Fig.13).

The flow rates of various capillaries were calibrated as a function of pressure drop by measuring the rate of rise of a soap bubble in a graduated glass tube of uniform cross section.

After the gases had been metered, they were passed through a mixing column of glass beads for uniform mixing before entering furnace. The gas mixtures entered at the bottom

of vertical reaction tube in which the test specimen was equilibrated to the ambient and exited at the top of the tube assembly.
The assembly consisted of a mullite tube to which were sealed pyrex standard taper joints on both ends.(Fig.14). The total gas flow rate was maintained at 0.8 cm/sec to prevent thermal diffusion.(36)

5-3. Electrical conductivity measurement.

A standard four-probe d.c. technique was employed for measurement. A rectangular sample was wrapped with four platinum wires. The spacing of the two inner-most wires,L, and sample cross-section area, A, were measured. The ratio(A/L) was used for conductivity calculation. A constant current was established by using a Keithley 225 current source and was supplied between the two outer wires while the voltage was measured across the inner-most wires, using a Keithley 191 digital multimeter.

The voltage measurement was made in both the forward and reverse directions and the average value was used for the calculation of conductivity. Ohmic contact to the sample was determined by measurement of the proportion-

ality of voltage with current increase for each sample.

The equilibrium state of the specimen was determined at the point where conductivity did not change after a specific length of time which depended on oxygen pressure and temperature.

6. EXPERIMENTAL RESULTS AND DISCUSSIONS.

6-1. Electrical conductivity of Cr-doped rutile.

The experimental data for Cr-doped rutile are shown in Fig.15-17. Doping levels were from 500-5000ppm. Pure rutile exhibits n-type semiconductor behavior in reducing atmospheres and in the present work a n-p transition at 900°C and 950°C(Fig.18) was observed in undoped rutile. For Cr-doping, a n-p transition is also observed for all doping levels, as expected, up to 1050°C. This is in agreement with the results reported for Al-doped rutile. (37) The experimental range of oxygen partial pressure is from 1 atmosphere to 10^{-19} atm.(at low temperature). With decreasing oxygen pressure, the conductivity shows two slopes of pressure dependence-approximately -1/5 at low pressure and -1/4 at medium pressure. Based on a point defect model with acceptor dopant(Tab.5-6), assuming the substitutional occupation of acceptor as shown in the ESR result(38), the slope of -1/5 at very low pressure is consistant with tetravalent titanium interstitials compensated by conductive electrons.
For the slope of -1/4, there are two possibilities-acceptors compensated by either divalent oxygen vacancies or tetravalent

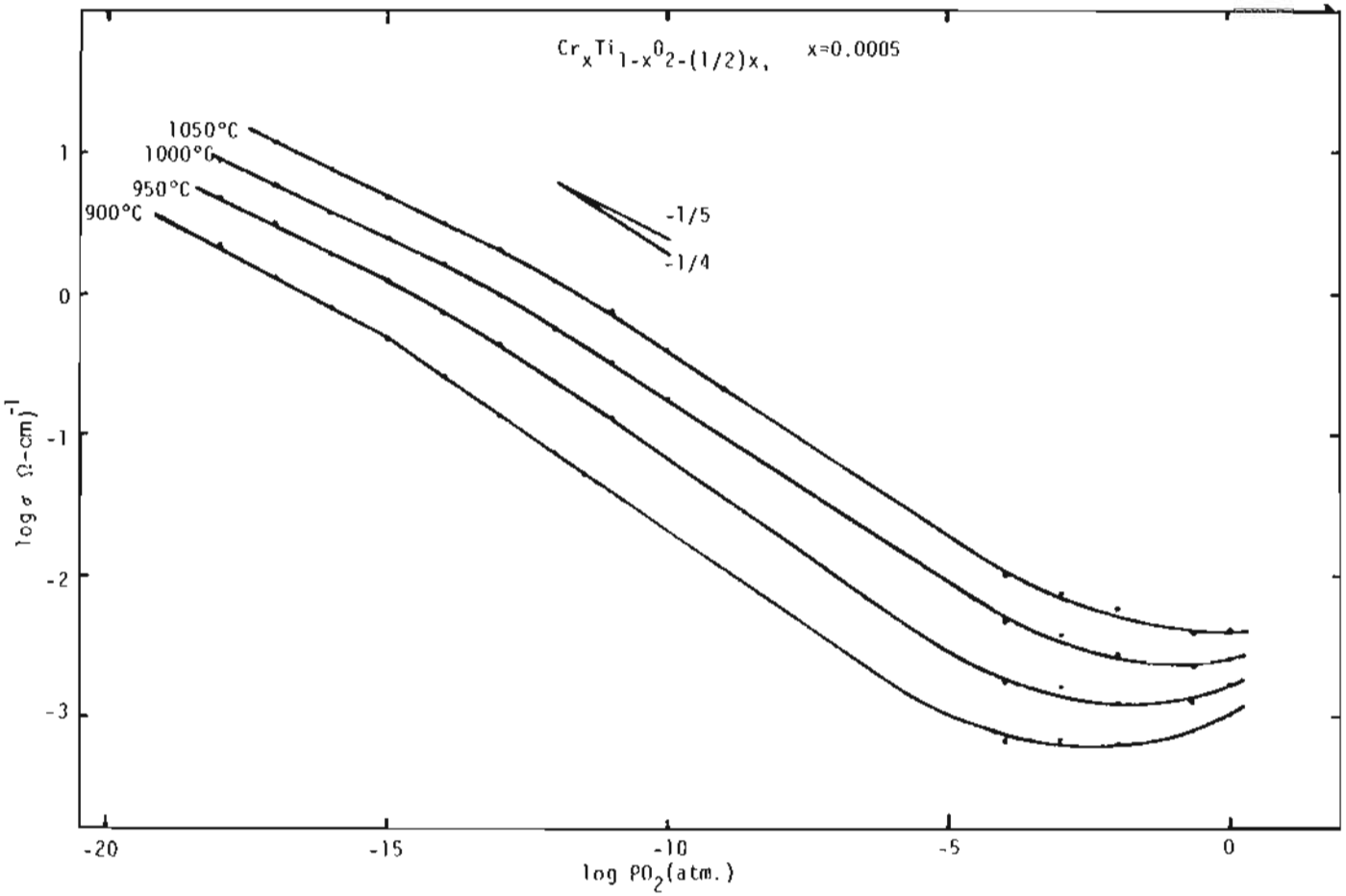

Fig.15. A plot of electrical conductivity of Cr-doped rutile vs oxygen pressure.

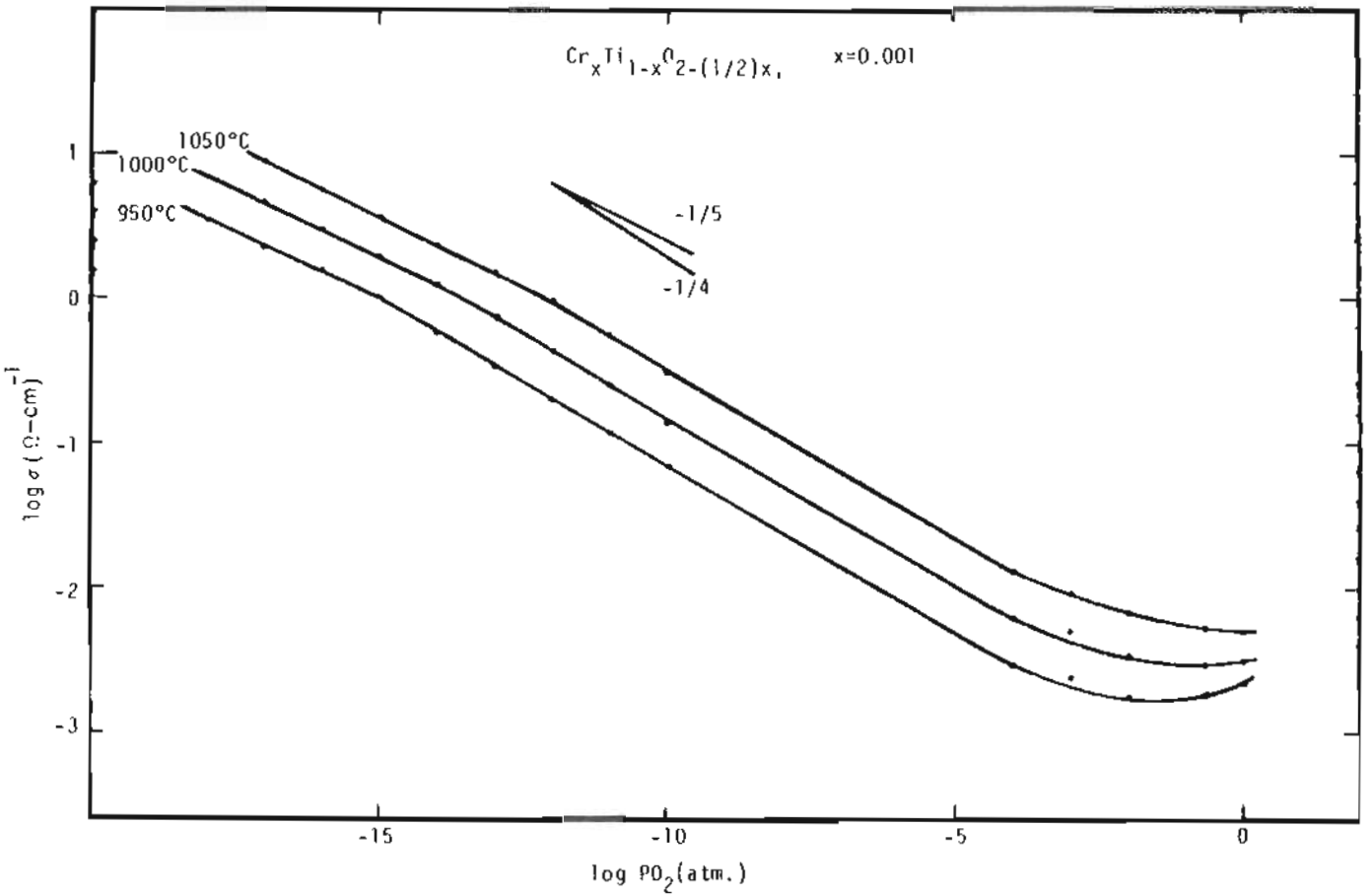

Fig.16. A plot of electrical conductivity of Cr-doped rutile vs oxygen pressure.

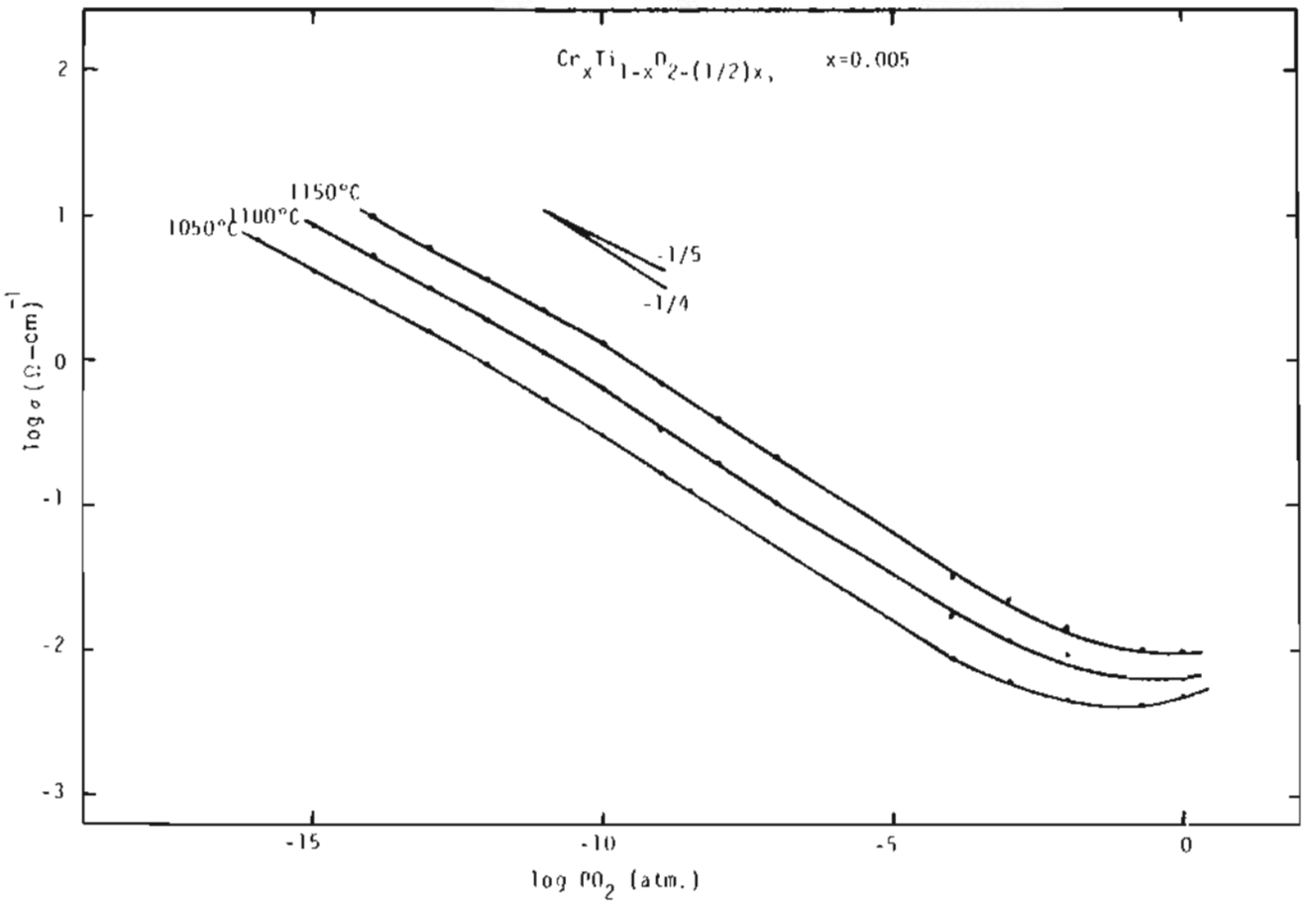

Fig.17. A plot of electrical conductivity of Cr-doped rutile vs oxygen perssure.

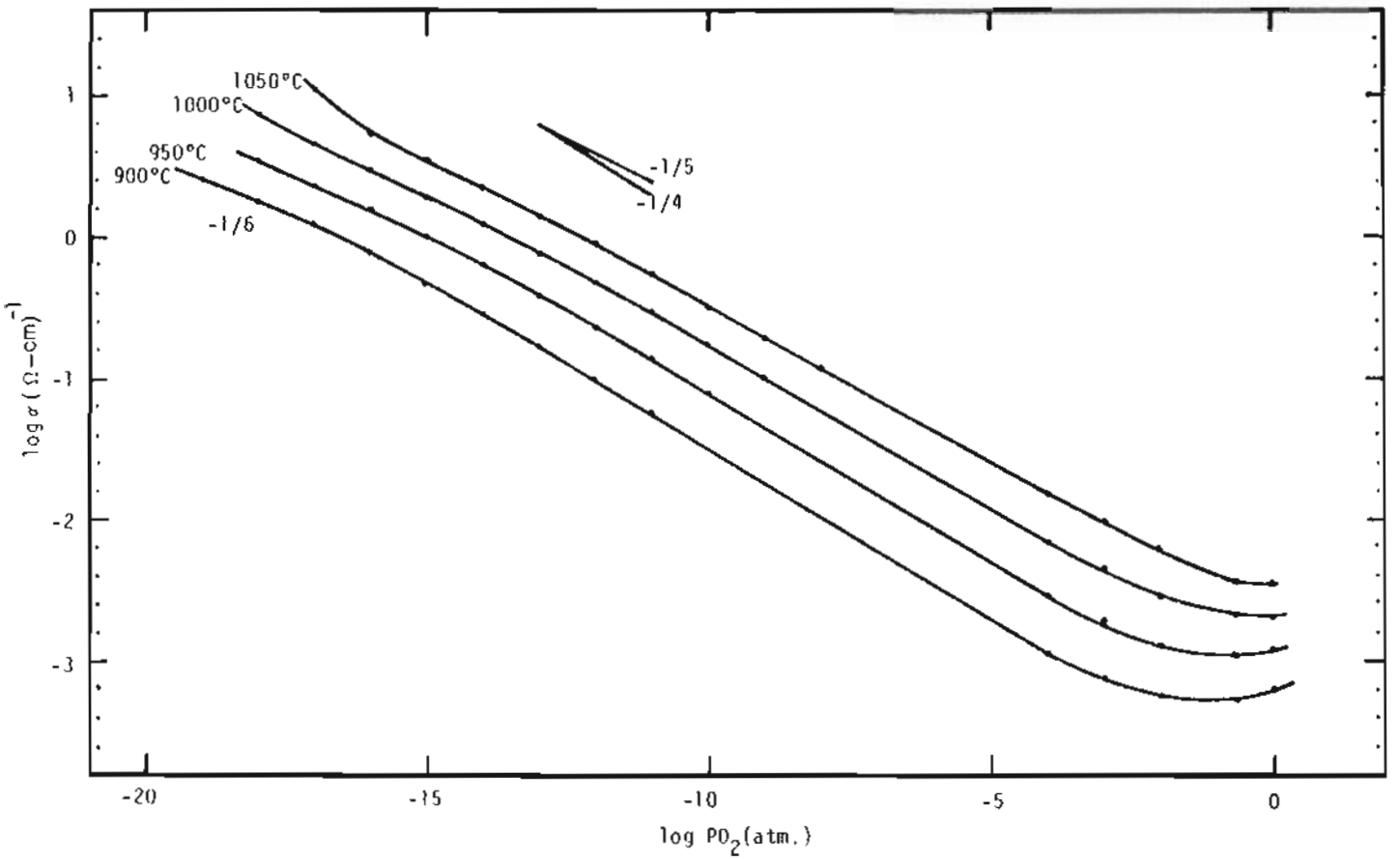

Fig.18. A plot of electrical conductivity of undoped rutile vs oxygen pressure.

titanium interstitials. For the slope of -1/5, combination of equations (8) and (9) with $\alpha=4$ leads to

$$TiO_2 \longrightarrow Ti_I + 4e' + O_2(g) \qquad -----(9')$$

$$K_4 = e^{-\frac{\Delta G_f}{RT}} = [Ti_I][n]^4 P_{O_2} \qquad -----(9")$$

When the electrical neutrality condition, $[n] \simeq 4[Ti_I^{4\cdot}]$, predominates

$$[n] = (4)^{1/5} P_{O_2} e^{-\frac{\Delta G_f}{5RT}}$$

The mobility of electrons is only a function of temperature and $\mu_e \propto \exp(-\Delta Gm/RT)$,(39) where ΔGm is the activation energy for electron migration.

According to equation(13) with Z=1 for electrons

$$\sigma \propto (4)^{1/5} q P_{O_2}^{-1/5} e^{-\frac{5\Delta G_m + \Delta G_f}{5RT}} \qquad ------(13')$$

Substituting the sum of energy term of the exponent with $\Delta G = \Delta H - T\Delta S$ and assuming that the variation of ΔS with temperature is negligible compared to the enthalpy change, equation(13') is simplified to

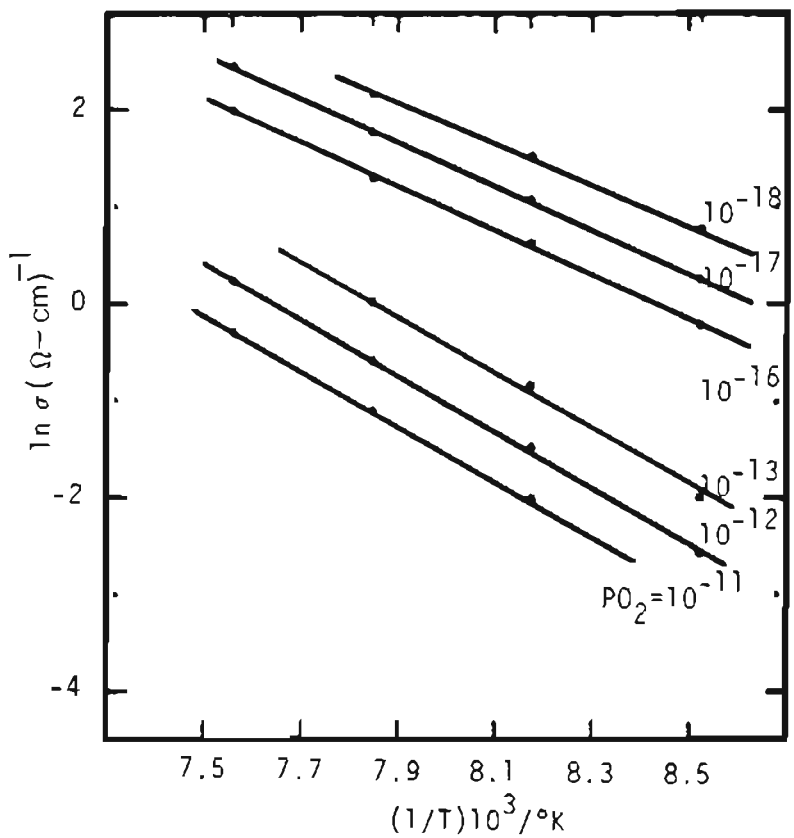

Fig.19. $\ln \sigma$ vs reciprocal temperature of Cr-doped rutile(x=0.0005).

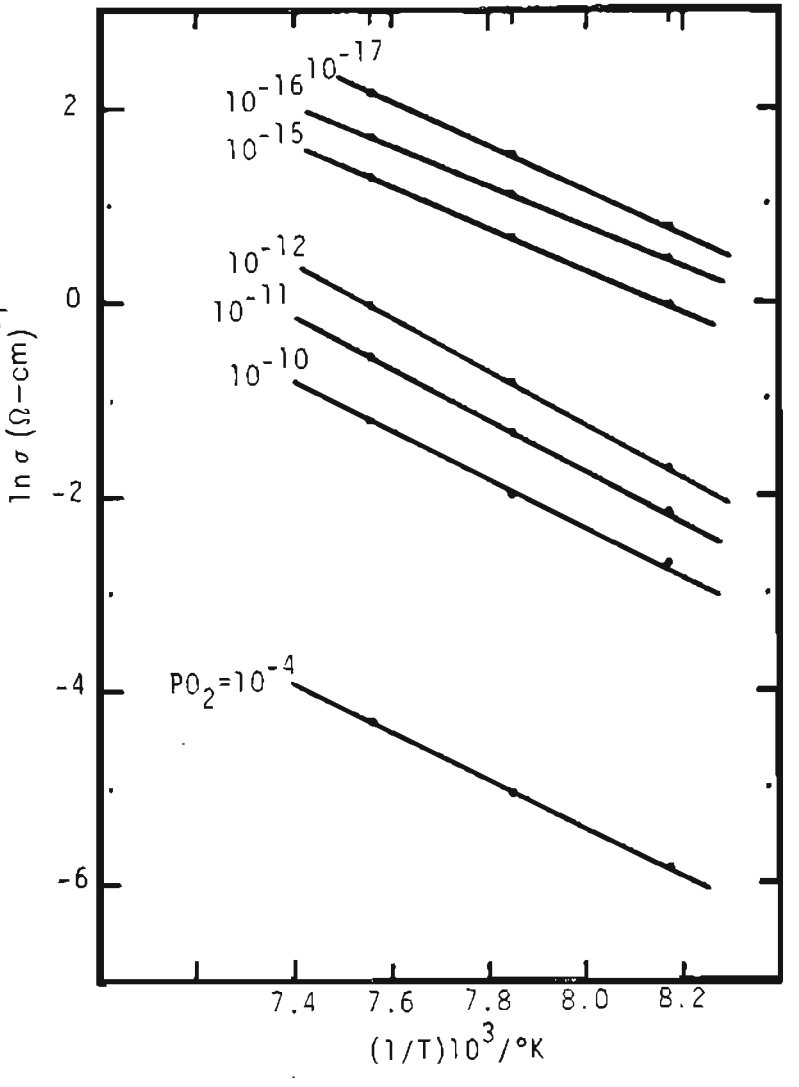

Fig.20. $\ln\sigma$ vs reciprocal temperature of Cr-doped rutile(x=0.001).

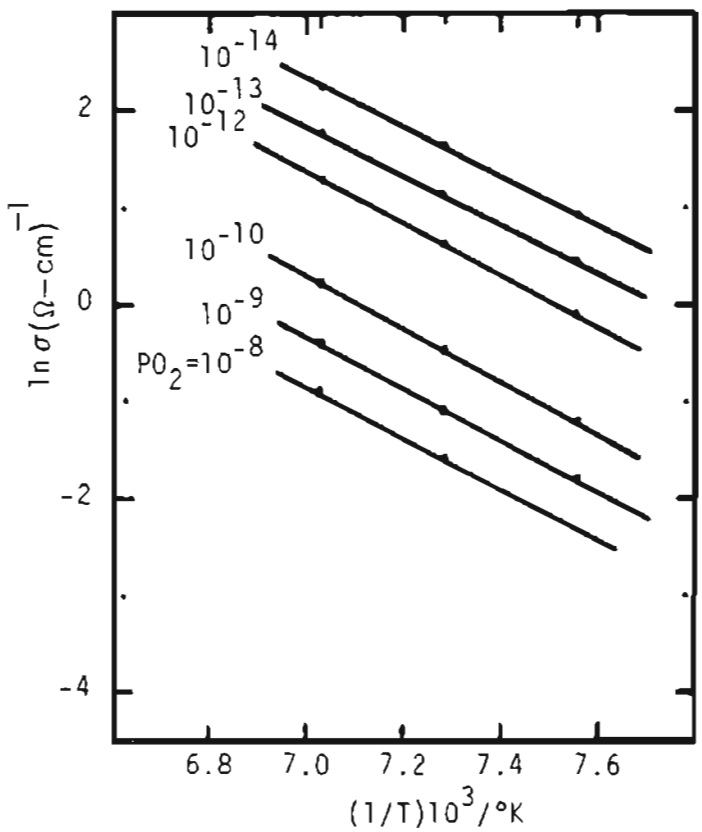

Fig.21. $\ln\sigma$ vs reciprocal temperature of Cr-doped rutile(x=0.005).

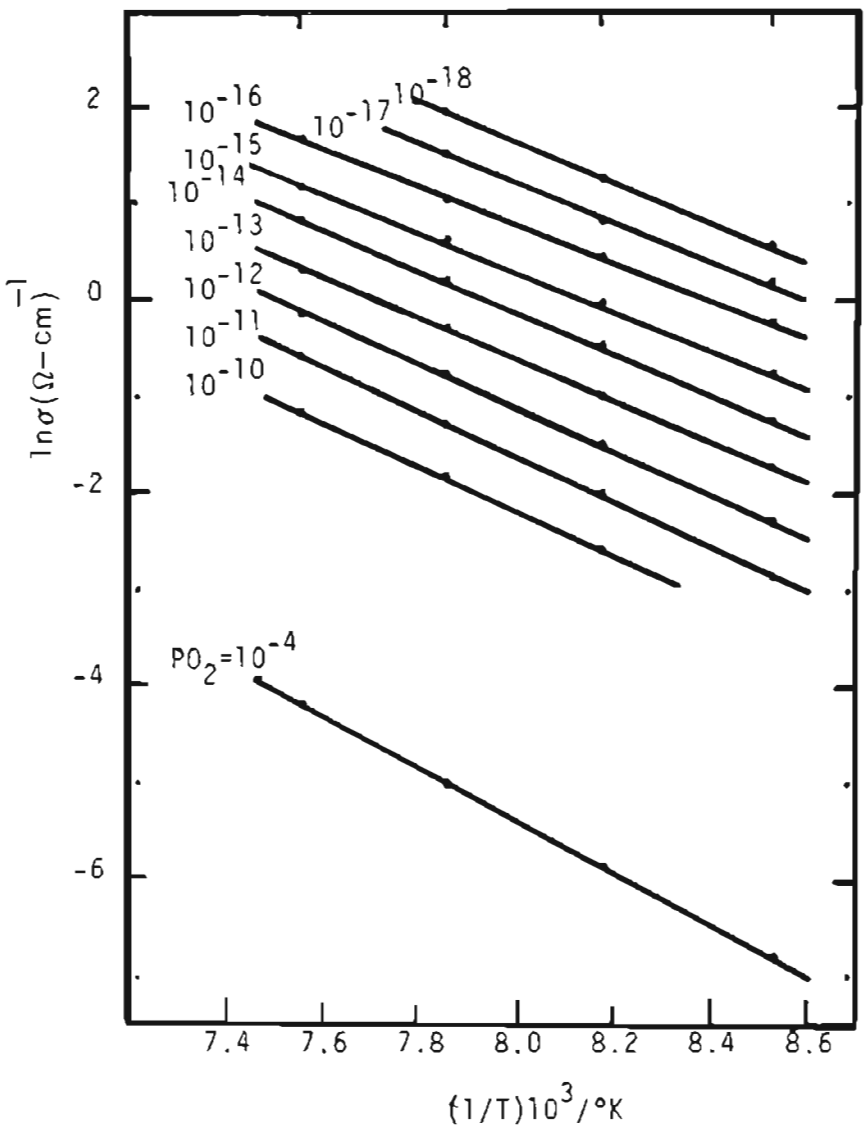

Fig.22. $\ln\sigma$ vs reciprocal temperature of undoped rutile.

$$\sigma \propto P_{O_2}^{-1/5} e^{-\frac{\Delta H}{5RT}} \qquad \text{------(13")}$$

ΔH is the arrhenius activation energy for conduction,which is approximately equal to the sum of $(5\Delta G_m + \Delta H_f)$.
By assuming that the electron mobility is proportional to exp(0.1/kT),(39) the standard enthalpy of formation of the reaction

$$TiO_2 \longrightarrow Ti_I^{4\cdot} + 4e' + O_2(g)$$

can be calculated from the arrhenius plots (Fig.19-22) and are tabulated in Table 9-11. The average activation energy for conduction is 9.9 eV (228.3Kcal/mol).
In the medium range of oxygen partial pressure, with the electrical neutrality condition, $2[V_O^{\cdot\cdot}] \simeq [M_{Ti}'] \simeq [M_{Ti}]_{tot}$. the reaction goes as equation(14), that is

$$Cr_2O_3 \xrightarrow{TiO_2} 2Cr_{Ti}' + 3O_O + V_O^{\cdot\cdot}$$

With the combination of (4),(5),and (6), the law of mass action leads to

$$K_O K_1 K_2 \simeq 1/2[M_{Ti}]_{tot} . P_{O_2}^{1/2} [n]^2 \qquad \text{-----(26)}$$

PO_2(atm.)	ΔH(Kcal/mole)	ΔH_f(Kcal/mole)
10^{-18}	209.1	197.6
10^{-17}	226.9	215.4
10^{-16}	226.9	215.4

Table 9. Arrhenius activation energies for conduction of 500ppm Cr-doped rutile for $\sigma \propto PO_2^{-1/5}$.

(ΔH_f; formation energy of corresponding reaction)

PO_2(atm.)	ΔH(Kcal/mole)	ΔH_f(Kcal/mole)
10^{-17}	229.9	218.4
10^{-16}	201.0	189.5
10^{-15}	213.9	202.4

Table 10. Arrhenius activation energies for conduction of 1000ppm Cr-doped rutile for $\sigma \propto PO_2^{-1/5}$.

PO_2(atm.)	ΔH(Kcal/mole)	ΔH_f(Kcal/mole)
10^{-14}	242.8	231.3
10^{-13}	242.8	231.3
10^{-12}	261.4	249.9

Table 11. Arrhenius activation energies for conduction of 5000ppm Cr-doped rutile for $\sigma \propto PO_2^{-1/5}$.

PO_2(atm.)	ΔH(Kcal/mole)	ΔH_f(Kcal/mole)
10^{-13}	118.6	114.0
10^{-12}	115.7	111.1
10^{-11}	109.3	104.7

Table 12. Arrhenius activation energies for conduction of 500ppm Cr-doped rutile for $\sigma \propto PO_2^{-1/4}$ (excess charge compensated by $V_O^{\cdot\cdot}$).

PO_2(atm.)	Δ H(Kcal/mole)	Δ H_f(Kcal/mole)
10^{-12}	109.3	104.7
10^{-11}	102.9	98.3
10^{-10}	98.4	93.8
10^{-4}	98.4	93.8

Table 13. Arrhenius activation energies for conduction of 1000ppm Cr-doped rutile for $\sigma \propto PO_2^{-1/4}$. (excess charge compensated by $V_o^{\cdot\cdot}$).

PO_2(atm.)	Δ H(Kcal/mole)	Δ H_f(Kcal/mole)
10^{-10}	106.8	102.2
10^{-9}	106.1	101.5
10^{-8}	108.7	104.5

Table 14. Arrhenius activation energies for conduction of 5000ppm Cr-doped rutile for $\sigma \propto PO_2^{-1/4}$ (excess charge compensated by $V_o^{\cdot\cdot}$).

which means $\sigma \propto P_{O_2}^{-1/4}$.

The experimental activation energies from $\log \sigma$ vs $1/T$ are shown in Table 12-14, and the average energy for conduction is 4.5eV(103.4Kcal/mol).

If the neutrality condition is $4[Ti_I^{4}] \simeq [M'_{Ti}] \sim [M_{Ti}]_{tot.}$ the reaction corresponds to equation(19).

$$2Cr_2O_3 + Ti_{Ti} \longrightarrow 4Cr'_{Ti} + Ti_I^{4\cdot} + 6O_o \quad ---(19\text{-}1)$$

With the combination of equations (8) and (9), it is obtained that

$$K_I K_4 \simeq 1/4[Cr_{Ti}]_{tot.}[n]^4 P_{O_2} \quad -----(27)$$

From equation (27), the energy of 9.37eV (216.0 Kcal/mol) is obtained (Table 15-17). This is close to that of reaction (9'). From the calculation oxygen vacancies are energetically more favorable than titanium interstitials. With increasing temperature the region of -1/5 dependence extends toward higher oxygen partial pressure.

Gautron et al(40) measured the electrical conductivity of acceptor and donor-doped rutile equilibrated at high temperature and quenched to room temperature. The electrical conductivity measurements were carried out at both room and high temperatures. For samples equilibrated at lower

PO_2(atm.)	Δ H(Kcal/mole)	ΔH_f(Kcal/mole)
10^{-13}	237.3	228.1
10^{-12}	231.3	222.1
10^{-11}	218.6	209.4

Table 15. Arrhenius activation energies for conduction of 500ppm Cr-doped rutile for $\sigma \propto PO_2^{-1/4}$ (excess charge compensated by $Ti_I^{4\cdot}$).

PO_2(atm.)	Δ H(Kcal/mole)	ΔH_f(Kcal/mole)
10^{-12}	218.6	209.4
10^{-11}	206.0	196.8
10^{-10}	196.8	187.6
10^{-4}	196.8	187.6

Table 16. Arrhenius activation energies for conduction for 1000ppm Cr-doped rutile for $\sigma \propto PO_2^{-1/4}$ (excess charge compensated by $Ti_I^{4\cdot}$).

PO_2(atm.)	Δ H(Kcal/mole)	Δ H_f(Kcal/mole)
10^{-10}	213.6	204.4
10^{-9}	212.2	203.0
10^{-8}	217.4	208.2

Table 17. Arrhenius activation energies for conduction of 5000ppm Cr-doped rutile for $\sigma \propto PO_2^{-1/4}$ (excess charge compensated by $Ti_I^{4\cdot}$).

pressures, the conductivity at room temperature is parallel to that reported at high temperature. This supports the theory that the intrinsic defects generated by reduction are dominant and the energy center of these defects is close to the conduction band. Therefore, high conductivity is maintained at room temperature. In the region of -1/4 slope at high temperature, the conductivity falls drastically at room temperature. This indicates that acceptors as impurities are dominant and conductive electrons at high temperature are trapped at the deeper levels of the acceptors when quenched to room temperature.

For undoped TiO_2, the conductivity dependence in the low oxygen pressure range is -1/6 at low temperature and becomes -1/5 with increasing temperature(Fig.18). Marucco et al(10) observed the same results. The dominant defects are divalent oxygen vacancies at low temperature and tetravalent titanium interstitials at high temperature. The spectral response measurements on ceramic TiO_2 prepared in a CO/CO_2 reducing atmosphere at 1400°C showed an abnormal wave shift of response between $P_{O_2}=10^{-7}$ and 10^{-9} atm of equilibrium pressure. This is interpreted as a change in the nature of the defect state from dominant oxygen vacancies to titanium interstitials.(41)

6-2.Electrical conductivity of Ta-doped rutile

The observed results for several doping levels are given in Fig.23-25. The conductivity dependence is characterized by three regions--a high pressure region where the slope is about -1/4, a medium pressure region of constant conductivity and a low pressure region in which the conductivity increases anomalously with reduction. Owing to the ESR results of Ta-doped rutile at low temperature(42) it is assumed that the Ta atom substitutes on normal titanium sites.

For the -1/4 slope of the high oxygen pressure region, the reaction follows equation(21)

$$2Ta_2O_5 \xrightarrow{TiO_2} 4Ta_{Ti}^{\cdot} + V_{Ti}^{4'} + 10\ O_O$$

and the excess charge of the donor is compensated by tetravalent titanium vacancies. Nb doping exhibited the same dependence in this region.(3)

The constant conductivity region is governed by reaction (22)

$$Ta_2O_5 \xrightarrow{TiO_2} 2Ta_{Ti}^{\cdot} + 2e' + 4O_O + 1/2\ O_2(g)$$

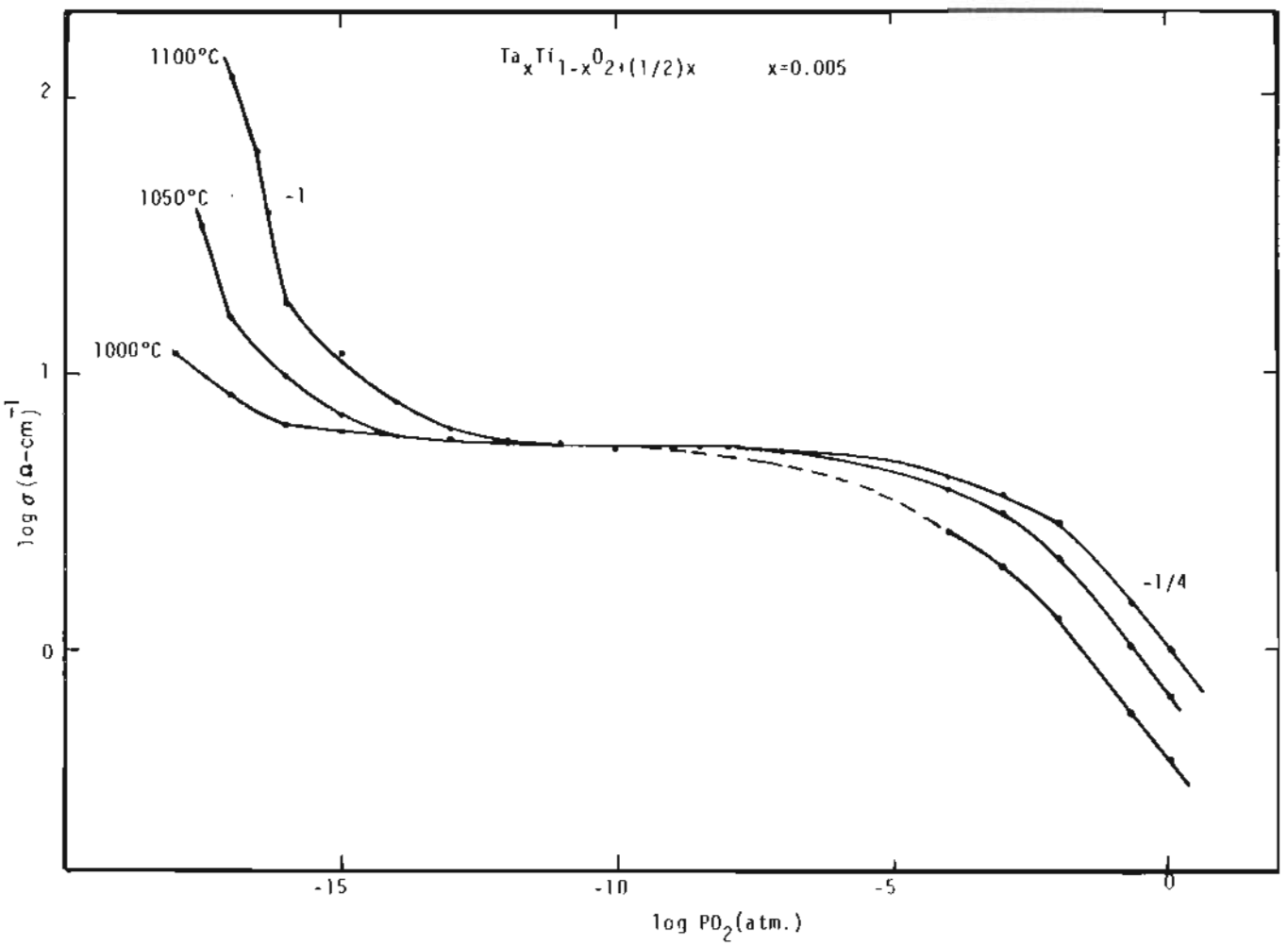

Fig.23. A plot of electrical conductivity of Ta-doped rutile vs oxygen pressure.

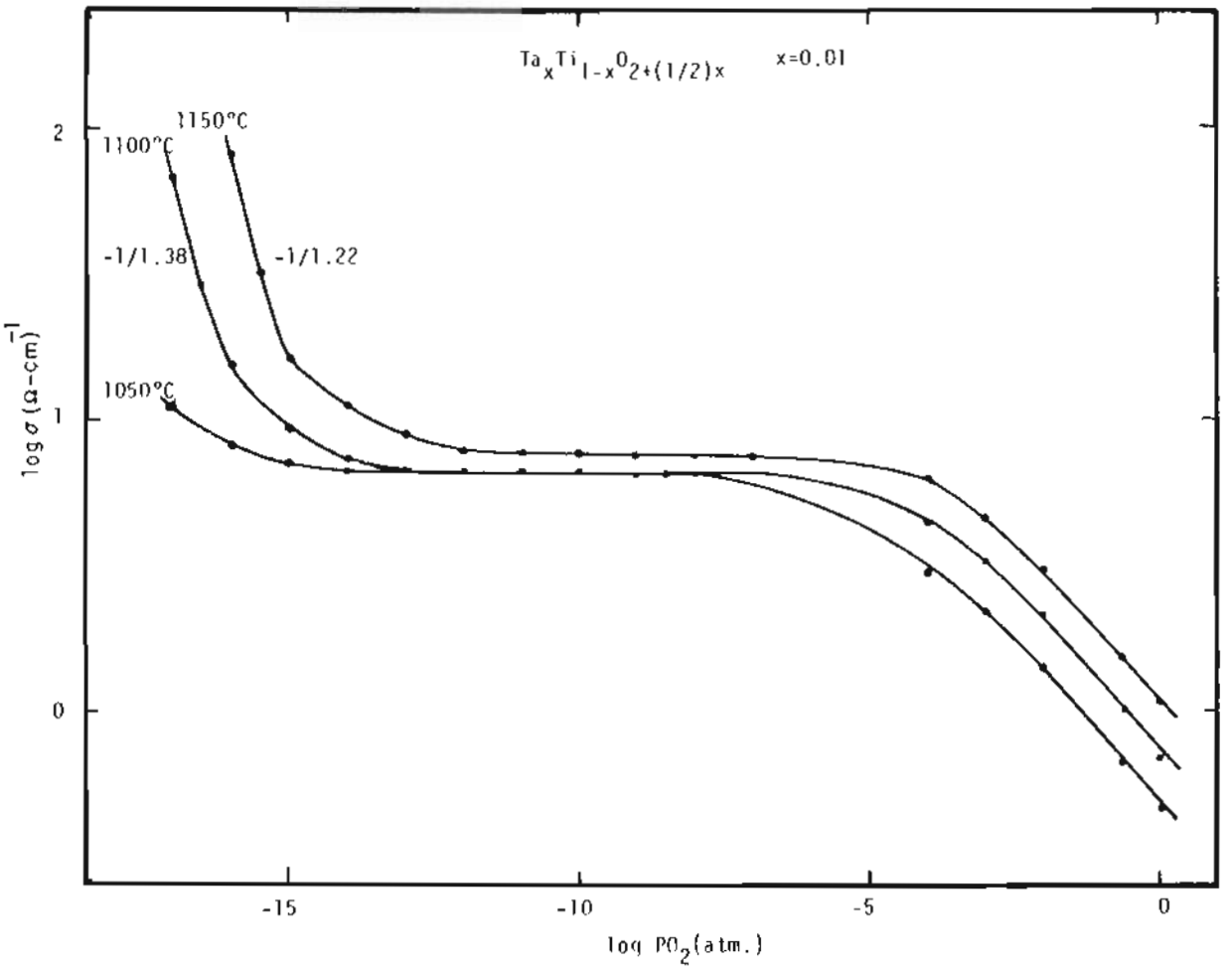

Fig.24. A plot of electrical conductivity of Ta-doped rutile vs oxygen pressure.

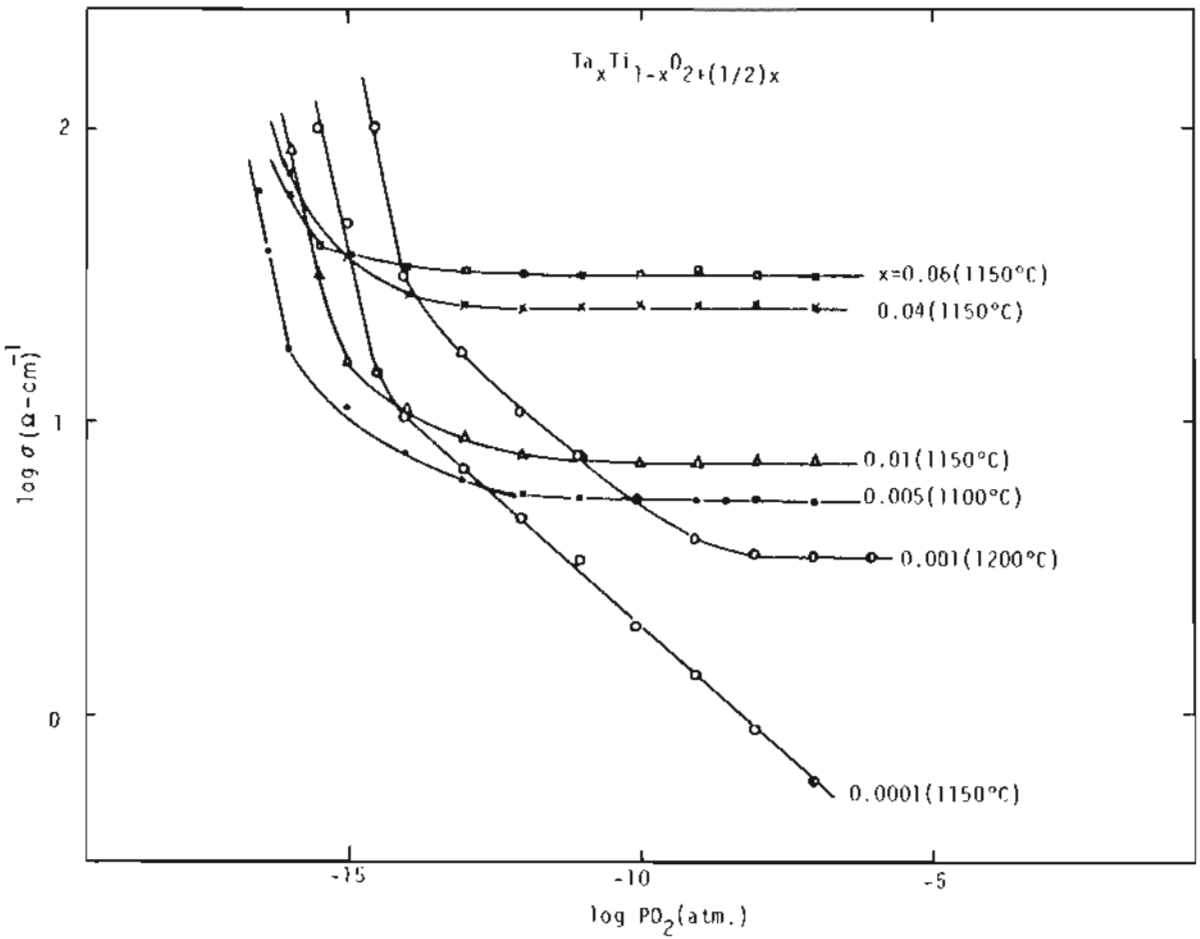

Fig.25. Plot of electrical conductivity of various doping levels of Ta-doped rutile vs oxygen pressure.

in which the excess charge of the donor is electronically compensated.

For a fixed doping level, the magnitude of conductivity does not vary with temperature within the experimental error range. Therefore, the donor is already exhausted at temperatures $>1000^{\circ}C$. This also indicates the electron mobility does not change with temperature.

According to Gautron et al, the conductivity of Nb-doped rutile at room temperature suddenly falls from constant conductivity with increasing oxygen partial pressure because of the deep energy level of the acceptor, tetravalent titanium vacancies. The same result is expected for Ta-doped rutile quenched to room temperature.

The conductivities at various levels of doping in the medium pressure region are shown in Fig.25. They show that the conductivity is entirely controlled by the doping level. For the ideal case of nondegeneracy in weak doping, the carrier density by ionized dopants is related to the doping level as

$$n_o = 1/2[(1+4N_d/n_1)^{1/2} - 1] \quad ----(A)[\text{Appendix 1}]$$

For weak doping($N_d << n_1$), the Fermi energy lies well below the energy center of the dopant and $n_o = N_d$. Therefore,

from equation (13)

$$\sigma = \mu_e e n_o \propto [N_d] \text{ ------(13')}$$

The conductivity is lineally proportional to the doping level. The experimental relationship of log σ vs log x of $Ta_xTi_{1-x}O_{2+x/2}$ is plotted in Fig.26. The overall relation is expressed as $\sigma = Ax^n$ with $A \simeq 2.24$ and $n=5/8$. Comparing the result with equation (13'), there is a contradiction in concentration dependence.

To correlate the observation with theory, the conductivity dependence is divided into segments b,and c. The linear b region is calculated for $A=2.62$ and $n \simeq 1$ which is linear between conductivity and concentration x. Segment c shows rather higher conductivity which may be influenced by uncounted impurities overcoming the dopant effect or there may be poor control of the doping level. Above segment b ($x>0.04$), the slope decreases ($n=5/8$). For strong doping ($N_d/n_1 >> 1$), $n_o \approx (N_d n_1)^{1/2}$ from equation (A) and the slope of n_o vs N_d decreases. The experimental result implies that for higher doping levels of Ta than $x=0.04$, the dopants are not exhausted and the conductivity increases with temperature.

The constant conductivity region is followed by the abrupt increase in conductivity with further reduction,

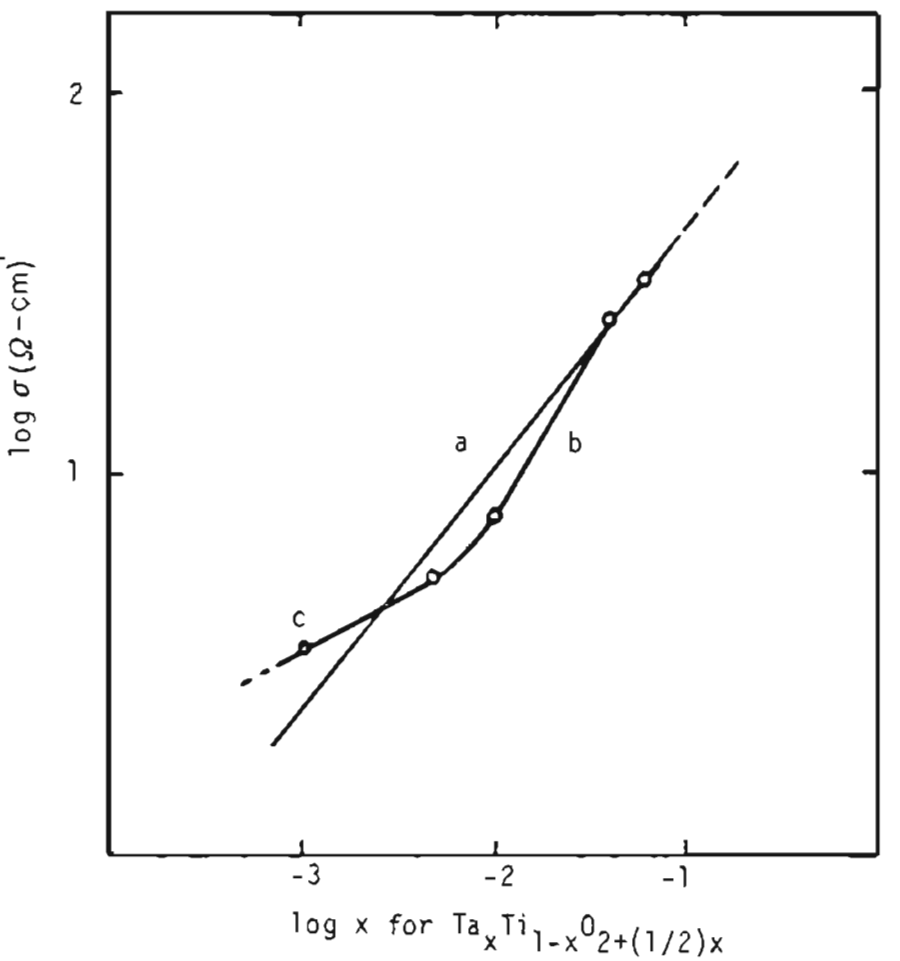

Fig.26. Dependence of conductivity as a function of doping levels in the medium range of oxygen pressure.(1100°C & 1150°C)

without an intrinsic -1/5 or -1/6 dependence between them. Beyond the transition region following the constant conductivity region, the slope of conductivity is between -1/1.0 and -1/1.4.

But at higher temperatures (1200°C, 1000ppm Ta in Fig.25), there is an intrinsic dependence region between the constant and abruptly increasing region. The intrinsic dependence is close to -1/6 for $10^{-13} < P_{O_2} < 10^{-10}$ atm. The undoped rutile also shows this abrupt increase of conductivity at high temperatures(>1050°C, Fig.27). The slope of -1/5 is followed by a sudden increase to -1/0.5 which is connected to a -1/2 slope region with reduction. Baumard et al observed similar step-variations in their experiments.(22) They attributed these anomalous behaviors to the existance of random crystallographic shear planes (132).

Generally for the -1/5 slope region, it has been interpreted by other investigators that titanium interstitials were the main defects (point defect model). But Baumard et al have shown that in the case of (132) CS planes as the main defect, the same slope can be obtained.(22)

Kröger discussed the effect of CS planes in the manner in which point defects determine the physical properties of shear structures such as conductivity,

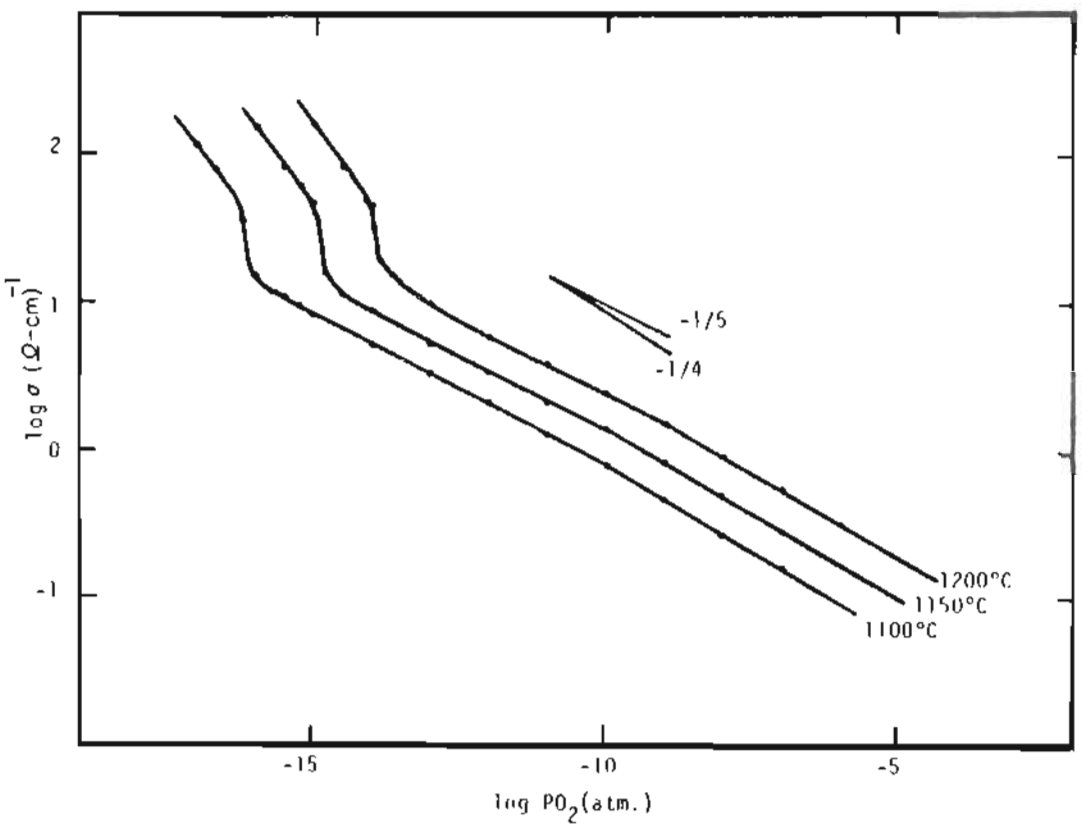

Fig.27. A plot of electrical conductivity of undoped rutile vs oxygen pressure at higher temperatures.

diffusion, EPR, etc.(43) He concluded that the existance of CS planes does not play a significant role when the amount of the CS planes is small. Therefore, the P_{O_2} dependence of these properties are the same as expected from a normal point defect model. Even with these conclusions, the point defect model cannot explain such a large slope of dependence as -1/0.5 to -1/2. A modified reaction model, which considers extended defects as well as point defects, can give an explanation for such an unexpected phenomenon.

Two reactions are considered for a new model--CS planes with oxygen vacancies or titanium interstitials as point defects.

(1). CS planes with oxygen vacancies

Further reduction of the already reduced state where only point defects exist causes interaction between CS planes and oxygen vacancies. During reduction the Ta dopant is assumed not to associate with CS planes which is reasonable because metal ions in CS planes requires lower valency.

The reaction is as follows,

$$Ta_yTi_{1-y}O_{2-x} \longrightarrow u(Ti_nO_{2n-1}) + Z/2\ O_2(g) + Ta_yTi_{1-y-nu}(V_{Ti}^{4'})_{nu}O_{2-x-u(2n-1)}(V_O^{\cdot\cdot})_{Z+u(2n-1)} + 2(Z-u)e' \quad ----(28)$$

Excess oxygen from the solid phase escape into the reducing atmosphere, leaving oxygen vacancies behind in the crystal.

As a result, the lattice potential energy increases and the crystal becomes unstable. Therefore (un) atoms of titanium participate to generate (u) moles of CS structure (Ti_nO_{2n-1}) leaving (un) atom moles of vacancies on Ti sites. Hence a 1:2 ratio of titanium and oxygen vacancies are eliminated from the rutile phase matrix through migration to the surface or grain boundaries. The simplified expression of the above reaction becomes

$$nTi_{Ti} + [(2n-1)+Z/u]O_O \longrightarrow Ti_nO_{2n-1} + Z/2u\ O_2(g) + (Z/u-1)V_O^{\cdot\cdot} + 2(Z/u-1)e' \quad ---(28')$$

Once the reaction (equation 28') reaches an equilibrium state, interaction between oxygen vacancies is assumed sufficiently small that the law of mass action can be applied. With the electrical neutrality condition, $[n] \simeq 2[V_O^{\cdot\cdot}]$

$$K = a_{cs}[V_o^{\cdot\cdot}]^{(Z/u-1)}[n]^{2(Z/u-1)}P_{O_2}^{Z/2u} \propto [n]^{3(Z/u-1)}P_{O_2}^{Z/2u}$$

where a_{cs} is the activity of CS planes and is approximated to be constant.

The electron concentration as function of oxygen partial pressure is expressed as

$$[n] \propto P_{O_2}^{-Z/[6(Z-u)]} = P_{O_2}^{-1/S} \quad \text{----(29)}$$

The reaction, equation (28′), implies that (Z/u) must be larger than unity to generate oxygen vacancies as well as CS planes. This is based on the thermodynamic assumption that CS planes as extended defects are generated from the point defect aggregation and the shear plane will be in equilibrium with point defects.(44) To explain this, reaction (equation 28′) can be expanded as follows;

$$nTi_{Ti} + [(2n-1)+Z/u]O_o \longrightarrow nTi_{Ti} + (2n-1)O_o + Z/2u\ O_2(g) + Z/u\ V_o^{\cdot\cdot} + 2Z/u\ e' \quad \text{-------(28-1)}$$

and

$$nTi_{Ti} + (2n-1)O_o + V_o^{\cdot\cdot} \rightleftharpoons Ti_nO_{2n-1} + 2\dot{h} \quad \text{-----(28-2)}$$

From equation(28-1)

$$K' \simeq P_{O_2}^{Z/2u}[V_O^{\cdot\cdot}]^{z/u}[n]^{2Z/u} \qquad \text{-----(28-3)}$$

From equation(28-2)

$$K'' \simeq \frac{a_{cs}[p]}{[V_O^{\cdot\cdot}]} \qquad \text{-----(28-4)}$$

Therefore

$$K'K'' \simeq a_{cs}P_{O_2}^{Z/2u}[V_O^{\cdot\cdot}]^{(Z/u-1)}[n]^{2Z/u}[p]^2 \qquad \text{----(28-5)}$$

Also since np=Ki

$$\frac{K'K''}{K_i^2} \simeq a_{cs}P_{O_2}^{Z/2u}[V_O^{\cdot\cdot}]^{(Z/u-1)}[n]^{2(Z/u\ -1)} \qquad \text{---(28-6)}$$

From this result equation (29) is obtained.

The possible values of S is limited in the range $0<S<6$. Table (18) lists some values of S, Z/u and the resulting ratio of crystallographic shear planes to oxygen vacancies. Z/u is the ratio of total oxygen escaping from the solid into the gas phase to the amount of oxygen vacancies which participate in the CS plane (ie, oxygen

S	Z/u	$CS/V_o^{\cdot\cdot}$
0	1/1	∞
1	6/5	5/1
1.2	5/4	4/1
1.5	4/3	3/1
2	3/2	2/1
3	2/1	1/1
4	3/1	1/2
5	6/1	1/5

Table 18. Values of S, corresponding Z/u, and ratios $CS/V_o^{\cdot\cdot}$.

vacancies eliminated by the generation of CS planes). For increasing S values, $CS/V_O^{\cdot\cdot}$ decreases and at S=6 no CS planes form. For undoped rutile, at very low oxygen pressures we observed a slope close to -1/6 at 900°C and -1/5 at 1200°C. The slope -1/6 is from oxygen vacancies as the dominant point defects.

(2) CS planes with titanium interstitials

For this case the reaction proceeds as follows

$$Ta_yTi_{1-y}O_{2-x} \longrightarrow u(Ti_nO_{2n-1}) + Z/2\ O_2(g) + Ta_yTi_{1-y-nu-(Z-u)/2}O_{2-x-u(2n-1)-Z}(Ti_I^{4\cdot})_{(Z-u)/2} + 2(Z-u)e' \quad ---(30)$$

This is simplified as

$$[n+ 1/2\ (Z/u -1)]Ti_{Ti} + [(2n-1)+ Z/u]O_O \longrightarrow Ti_nO_{2n-1} + Z/2u\ O_2(g) + 1/2\ (Z/u -1)Ti_I^{4\cdot} + 2(Z/u -1)e' \quad --(30')$$

Assuming a fixed activity of CS planes and the electrical neutrality condition, $4[Ti_I^{4\cdot}] \cong [n]$, it follows that

$$[n] \propto P_{O_2}^{-Z/[5(Z-u)]} = P_{O_2}^{-1/S'} \quad \text{-----(31)}$$

The S'values are limited to the range $0<S'<5$ for generation of CS planes. Table 19 shows various S' and corresponding ratios of Z/u and $CS/Ti_I^{4\cdot}$.

According to the present model, the abrupt change of conductivity at very low oxygen partial pressures is solely attributed to the variation of concentration of charge carrier through the reaction of equations (28) or (30). It should also be noted that a combination of oxygen vacancies with CS planes can also cause the observed -1/5 dependence of conductivity at low oxygen partial pressure.

The reactions, equation (28') and equation (30'), are also applicable to the undoped rutile for the equilibrium between CS planes and point defects. This is evident from the derived equations (28') and (30').

It is believed that donor or acceptor impurities shift the oxygen pressure where both the extended and point defects become stable through lattice potential stability. However the experimental observation of the variation of oxygen pressure between the undoped and Ta-doped cases is small. For example, for T=1150°C, the abrupt change of conductivity in undoped rutile occurs

S′	Z/u	$CS/Ti_I^{4\cdot}$
0	1/1	∞
1	10/8	8/1
1.2	25/19	19/3
1.5	20/14	14/3
2	5/3	3/1
3	10/4	4/3
4	5/1	1/2

Table 19. Values of S′, corresponding Z/u, and ratios $CS/Ti_I^{4\cdot}$.

at $P_{O_2}=10^{-14.5}$ atm., while for 1% Ta-doped rutile the change is at $P_{O_2}=10^{-15}$ atm.. At T=1100°C the undoped sample shows the abrupt change at $P_{O_2}=10^{-16}$ and approximately the same pressure for the doped sample of 0.5% Ta. For the Ta-doped sample it is observed that there occurs a wide range of transitions prior to the sudden increase of conductivity which is absent in the undoped sample. The abrupt increase of conductivity dependence after the -1/5 region (Fig.27) is interpreted as a biphasic region consisting of dispersed CS planes within a rutile matrix. The upper composition limit of the CS plane is $TiO_{1.973}$ at 1000°C which corresponds to the (132) CS plane. This abrupt slope is close to 2.0, being followed by the -1/2 slope region for undoped and ~1 to ~1/1.4 for the Ta-doped rutile.

All of these large slope dependences are interpreted by the new model presented here.

For the broad transition range from the pressure independent region of conductivity to the anomalously steep region for the cases of Ta-doped rutile, it was not investigated whether this is caused by generation of CS planes or a short range of intrinsic dependence.

Observations in the electron microscope support the presence of extended defects for very small departures

from stoichiometry, as low as $10^{-3} \sim 10^{-4}$. To accept this observation, there are several other phenomena still remaining to be explained, such as the variation of chemical diffusion coefficiant, and the hysteresis of oxygen chemical potential in different oxygen pressures.(11)

If, however, the extended defect occurs in the oxygen pressure range where the point defect model has been applied to interpret the data, a new model is required for this interpretation.

According to the conclusion made by Baumard et al from conductivity measurements, the equlibrium between TiO_{2-x} (mainly point defects) and the highest ordered phase Ti_nO_{2n-1} (extended planar defect in the rutile matrix) should occur at a larger departure from stoichiometry.

T.E.M. studies were conducted to confirm the range where the generation of extended defects occurs in Ta-doped rutile. These results were correlated with the observed electrical conductivity behavior.

7. T.E.M. STUDIES.

The crystallographic shear mechanism eliminates point defect by changing the mode of linkage of the TiO_6 octahedra. This results in restored coherence to the oxygen sublattice but creates a fault on the metal sublattice such as CS planes.

When an electron wave is passing through the crystal the fault plane causes a phase shift and image contrast occurs (Appendix 2.). A planar fault which is inclined with respect to the surface of the specimen shows up as a series of fringes. The properties of these fringes are determined by the value of the phase factor $\alpha = 2\pi g \star R$ which modifies the transmitted and diffracted intensities at the bottom of the crystal relative to their values for a perfect lattice at the top.

For fringe profiles there are two special cases, i.e. α-fringes and δ- fringes. α-fringes occurs when $\alpha = 2\pi g \star R \neq 0$ and $S_1 - S_2 = 0$. S_1 and S_2 are the deviation vectors on either side of the boundary. δ-fringes occur when $\alpha = 0$ and $W_1 - W_2 \neq 0$, where W is a dimensionless parameter with W=S*(extinction distance) which is used for the deviation from Bragg's condition.

The results of fringes for each of these cases in compara-

tively thick sections are listed in Appendix 3.
Translation interfaces such as antiphase boundaries (APB) and stacking faults produce α-fringes and twin interfaces result in δ-fringes.
By observing the symmetry of the outer fringes in bright and dark field images, we can analyse the family of crystallographic planes. When $\alpha = \pi$, the fringes in B.F. and D.F. images are complementary with respect to the background and the central fringe is bright in B.F. and dark in the D.F. image.
The diffraction pattern containing thin planar faults exhibit streaks perpendicular to the fault plane on the reciprocal lattice points when the fault plane is parallel to the incident beam. The supperlattice reflections by the ordered CS planes lie along the g vector of the planes and are closely spaced with strong reflections close to the rutile positions.(47)

7-1. SAMPLE PREPARATION.

Ta-doped(5000ppm) polycrystalline and undoped single crystal were annealed at two equilibrium states; in $P_{O_2} = 10^{-9}$ atm. and $10^{-16.5}$ atm. at 1100°C. The specimens were then atmosphere-quenched by pulling them from the

hot zone to room temperature in the controlled atmosphere furnace tube.

Fracture flakes crushed between two glass slides were mounted on a copper grid and carbon-coated. The mounted samples were examined in both Hitachi HU-11B-3 type microscope operated at 100 and 125 KV, and H-800 at 200KV.

7-2. T.E.M. ANALYSIS.

The interesting defects in the analysis are the CS planes to which the abrupt increases in electrical conductivity during reduction at low oxygen activity have been attributed. The representative planes observed in all samples treated in two different conditions are shown in Fig.T-1. Among these,(b),(c), and (d) are the very common defect planes observed.
In (a), planes (A) are wedge-shaped because they are not completely parallel to the electron beam direction, while planes (B) are nearly edge-on. These planes sometimes moved perpendicularly under the electron beam, until a certain density had been reached.

Plane (A) in (b) is clearly recognized as a twin plane from the intersection of two planes (A) and (B). Alternating twin bands are shown in (c) and (d) which are very common in all samples.

(1). Samples reduced at $P_{O_2}=10^{-9}$ atm.

In both doped and undoped samples, twin bands are observed. Besides these, {101} fault planes are observed as shown in Fig.T-2.

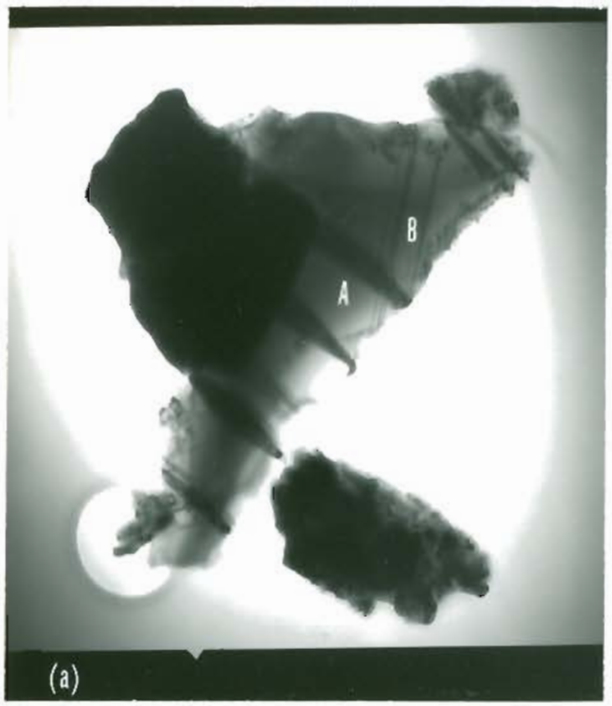

Doped sample reduced at 1100°C, $P_{O_2}=10^{-9}$atm. Antiphase boundaries.

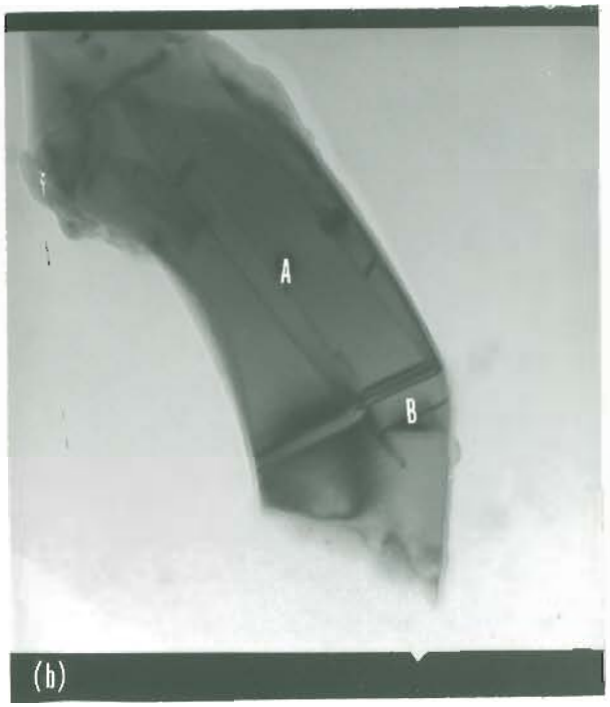

Doped sample reduced at 1100°C, $P_{O_2}=10^{-16.5}$atm. Twin plane.

Fig. T-1. Antiphase boundaries and twin planes observed commonly in the reduced samples(a-d).

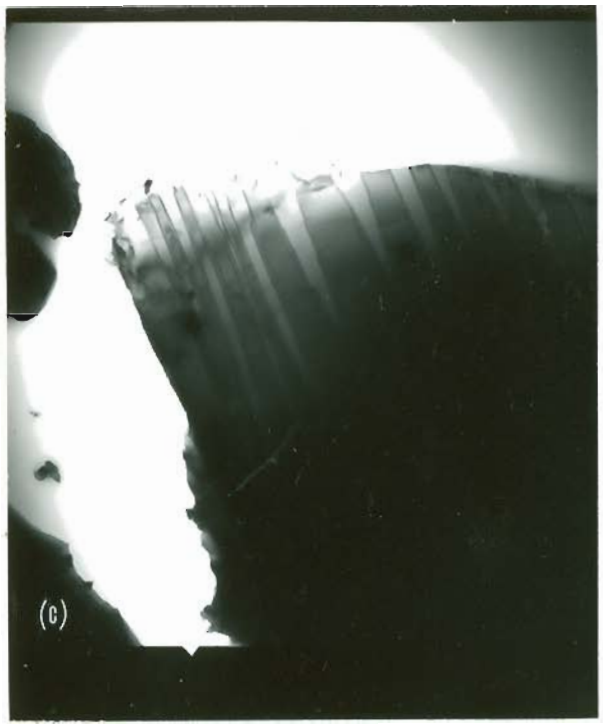

Doped sample reduced at 1100°C, $P_{O_2}=10^{-16.5}$atm. Twin bands.

Undoped sample reduced at 1100°C, $P_{O_2}=10^{-16.5}$atm. Twin bands.

It has been reported that the displacement vector R, in Cr-dope and undoped rutile, is 1/2 $\langle 011 \rangle_r$.(32,47). For the Ta-doped rutile, it is assumed R=1/2 $\langle 011 \rangle_r$ because the doping level is very low. The shear plane (101) is parallel to the displacement vector 1/2 $[\bar{1}01]$. Therefore, there is no perpendicular component of R on the plane (101). This plane doesn't cause any change in chemical composition which means the (101) plane is an antiphase boundary(APB). (a) in Fig.T-2 shows a heavy density of APB. Planes (b) in Fig.T-2 are (101) twin planes rather than APB. The diffraction pattern of (b) indicates as unsplit row of spots along $g(\bar{1}01)$ and all other spots are split in the direction parallel to the unsplit row. The planes are reflection twins. In pure single crystals, both APB and twins are observed as in the doped sample. No CS planes were observed in these samples. Therefore, nonstoichiometry by reduction at this oxygen partial pressure is achieved by point defects.

Bursill and Hyde reported APB{101} with R=1/2 $\langle 101 \rangle_r$ as a result of the operation of slip to release the elastic stress during reduction or possibly quenching.(32) Gibbs et al observed {101}twins in the slightly doped rutile with less than 5 mole % $CrO_{1.5}$ and equilibrated at 1330° K-1570° K in air.(51)

(a) Bright field of APB planes(101).

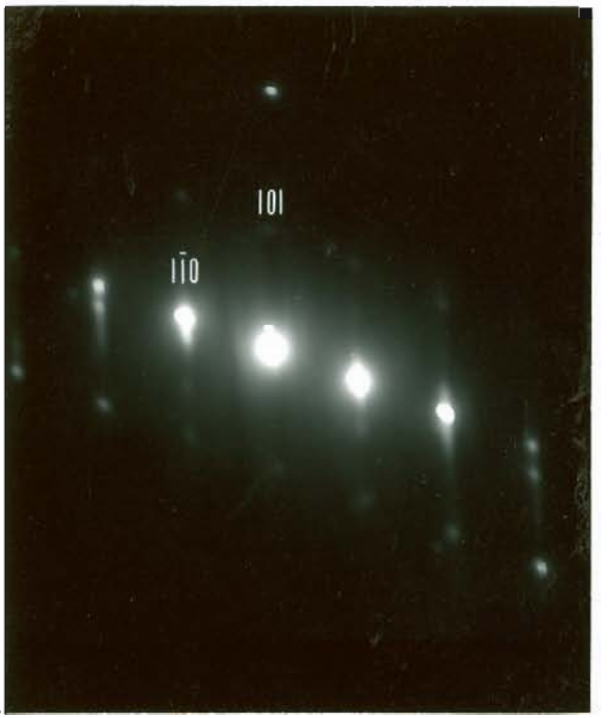

Diffraction pattern of APB planes, [$\bar{1}$11] zone axis.

Fig. T-2. Bright field images and SADs of twin and APB planes of doped(a,b) and undoped(c,d) samples reduced at 1100°C, $P_{O_2}=10^{-9}$atm.

(b) Bright field of twin planes($\bar{1}01$).

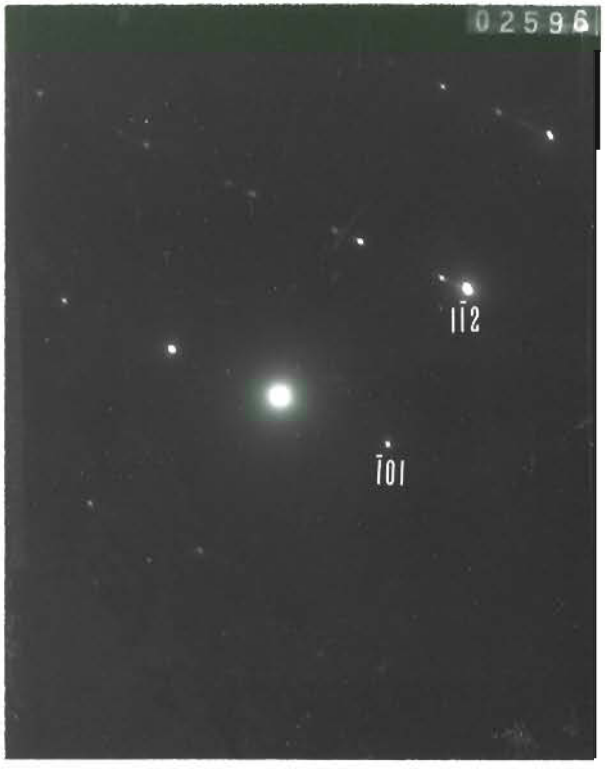

Diffraction pattern of reflection twin, [131] zone axis.

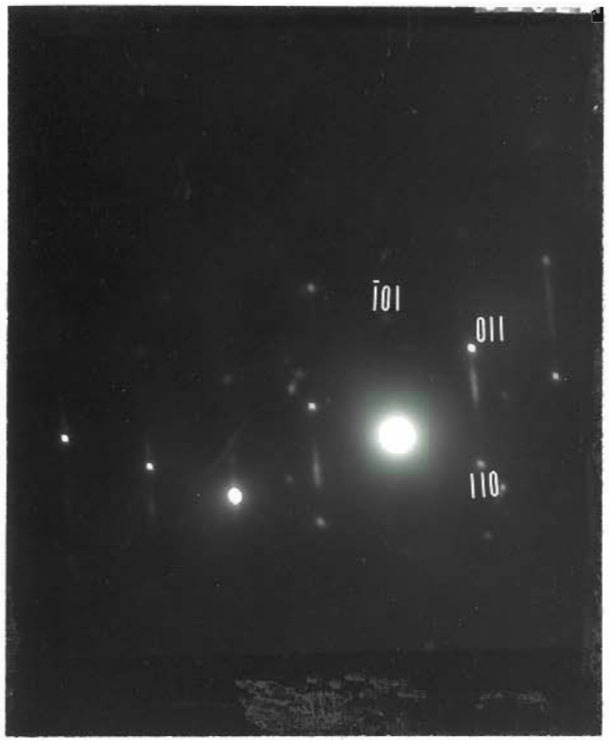

(c) Bright field and diffraction pattern of APB planes($10\bar{1}$), [$1\bar{1}1$] zone axis.

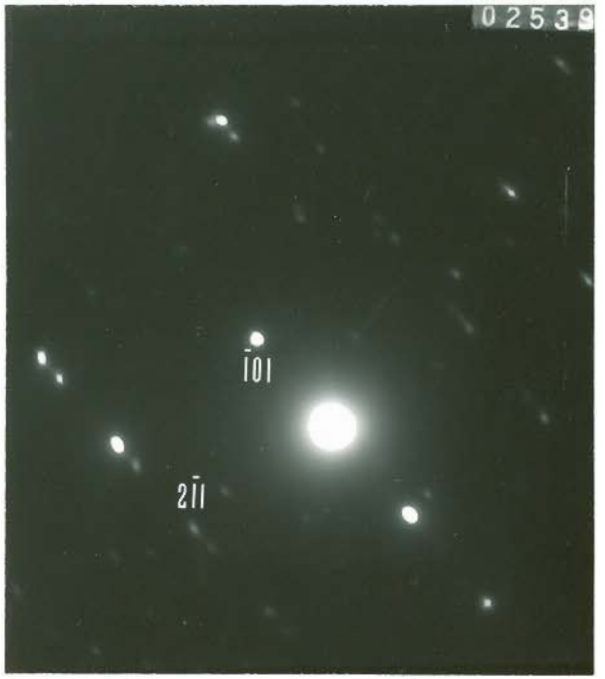

(d) Bright field and diffraction pattern of twin planes($\bar{1}01$), [131] zone axis.

(2). Samples reduced at $P_{O_2}=10^{-16.5}$ atm.

The selected area diffraction (SAD) patterns of undoped and doped samples of several crystal orientations are shown in Fig.T-3 and 4. After the samples were reduced in $P_{O_2}=10^{-9}$ atm., they exhibited considerable twinning. In addition to these planes, CS planes were observed. The occurence of CS planes was much less than that of the twin planes.

In both samples {132} and {121} CS planes were observed and the superlattice spots are very regular along the planar fault g vector. Higher magnification of the bright field (Fig.T-5) shows regular spacing of {121} CS planes. The spacing is approximately 19Å from both the bright field measurement and the calculation from the diffraction pattern. Some twins contain CS planes as shown Fig.T-5.

The reducing environment of these samples corresponds to the region of steep slope dependence of conductivity (Fig. 23.and 27.). The crystals reduced in this region contain CS planar faults as extended defects which are equilibrated with point defects according to equation (28-2). The ratio of the amount of these two types of defects depends on the reduction temperature (equation 28-4). The point defect model does not give the larger slope dependence of conductivity such as -1/2.

The combination of extended and point defects predicts the very large slopes of the measured electrical conductivity as a function of oxygen activity.

The TEM observation is consistent with the reaction model for the very low oxygen activity region where the extened defect exists in equilibrium with point defects to account for the abrupt increase in conductivity dependence. No extended defects are observed in the pressure independent conductivity region as expected by the new reaction model.

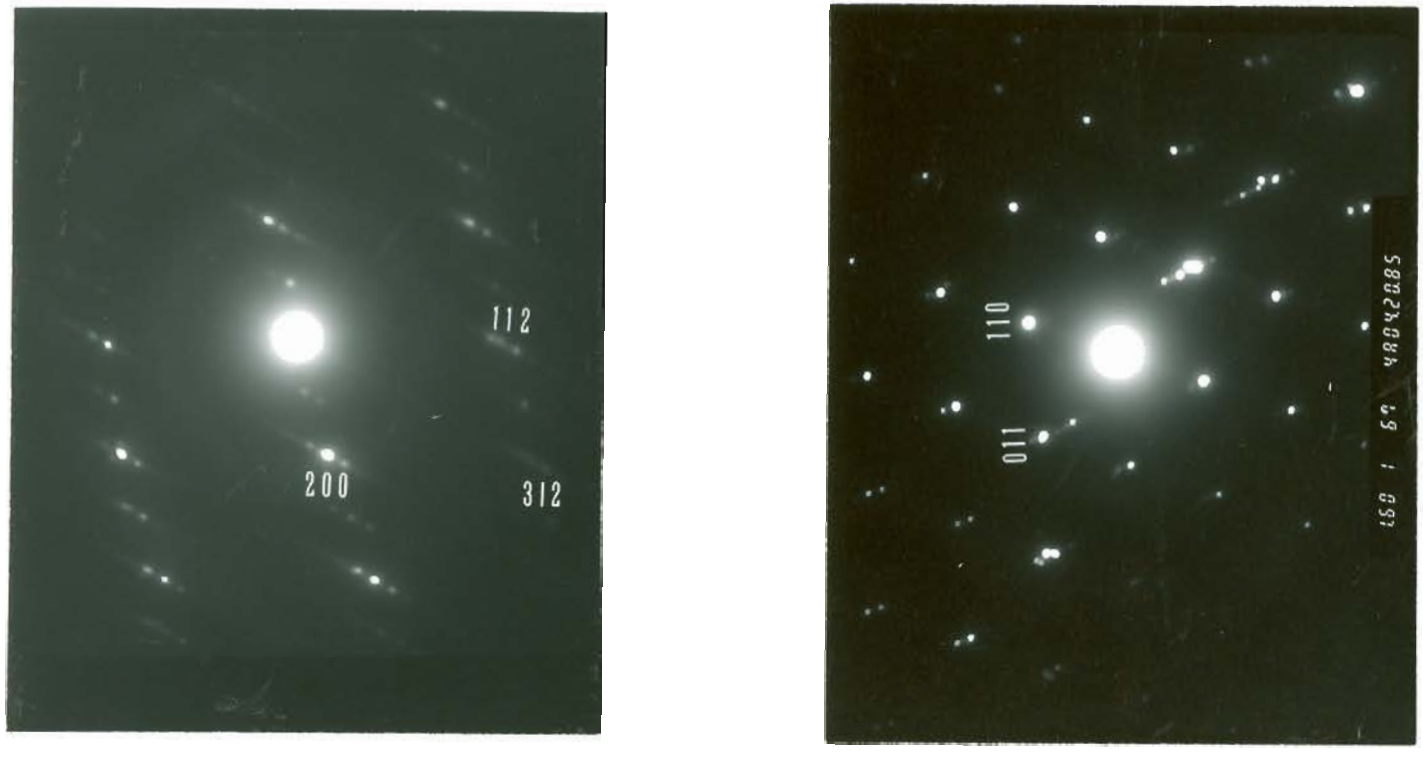

(a) (b)

Fig. T-3. SAD of various orientations of undoped sample reduced at 1100°C, $P_{O_2}=10^{-16.5}$ atm. Diffraction patterns showing supperlattice directions along [312](a; zone axis close to [02$\bar{1}$]), [121](b; zone axis close to [1$\bar{1}$1]), [101] and [01$\bar{1}$](c; zone axis close to [$\bar{1}$11]). CS planes (312)(a) , (121)(b) and {101} twins(c).

(c)

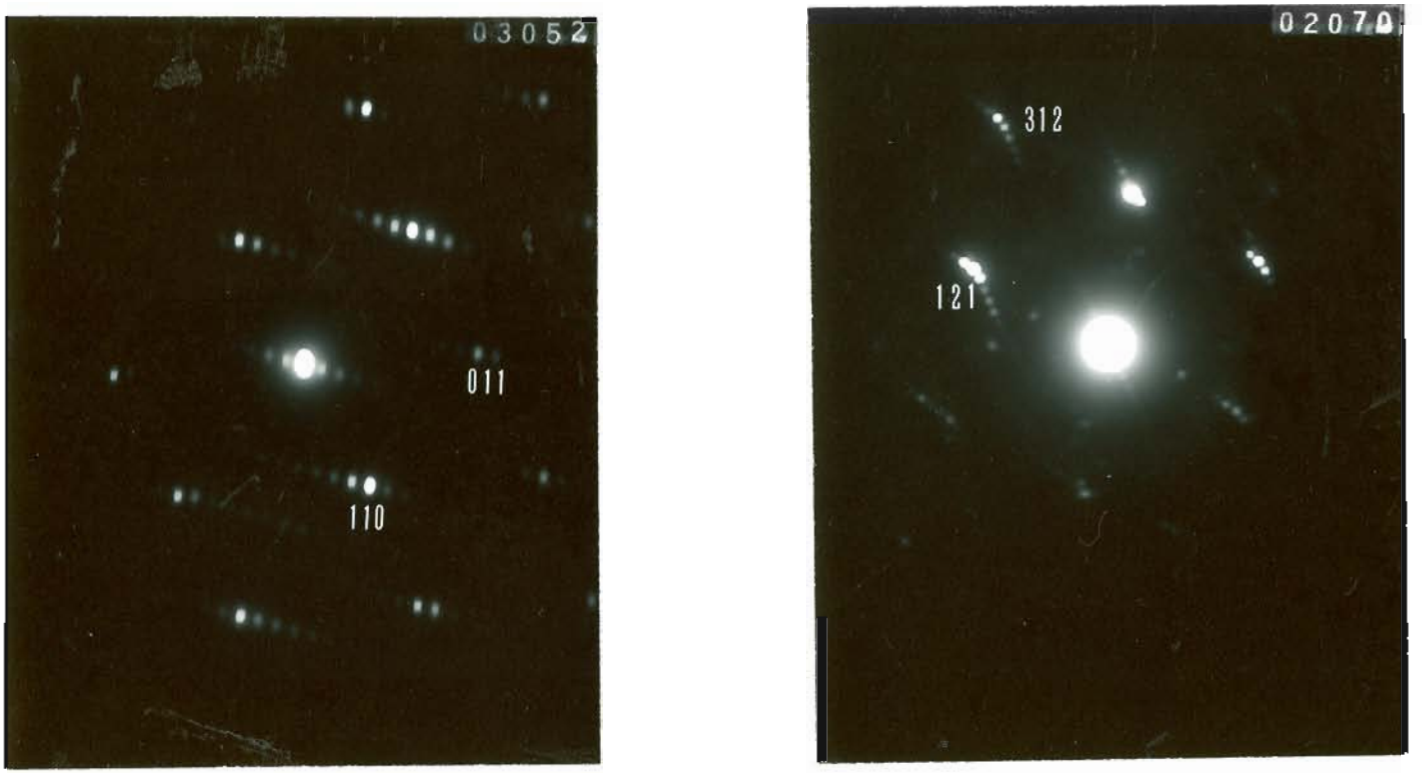

(a) (b)

Fig. T-4. SAD of various orientations of doped sample reduced at 1100°C, $P_{O_2}=10^{-16.5}$ atm. Diffraction patterns showing supperlattice directions along [132](a; zone axis[$1\bar{1}1$]), [312] and [121](b; zone axis[$31\bar{5}$]), and [$2\bar{1}1$](c; zone axis[$1\bar{1}\bar{3}$]). All are CS planes{121} or {132} .

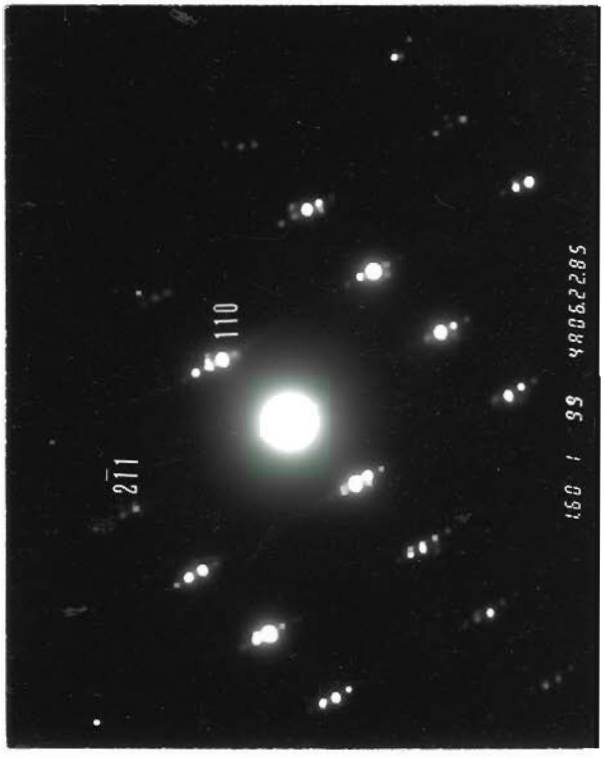

(c)

(a)

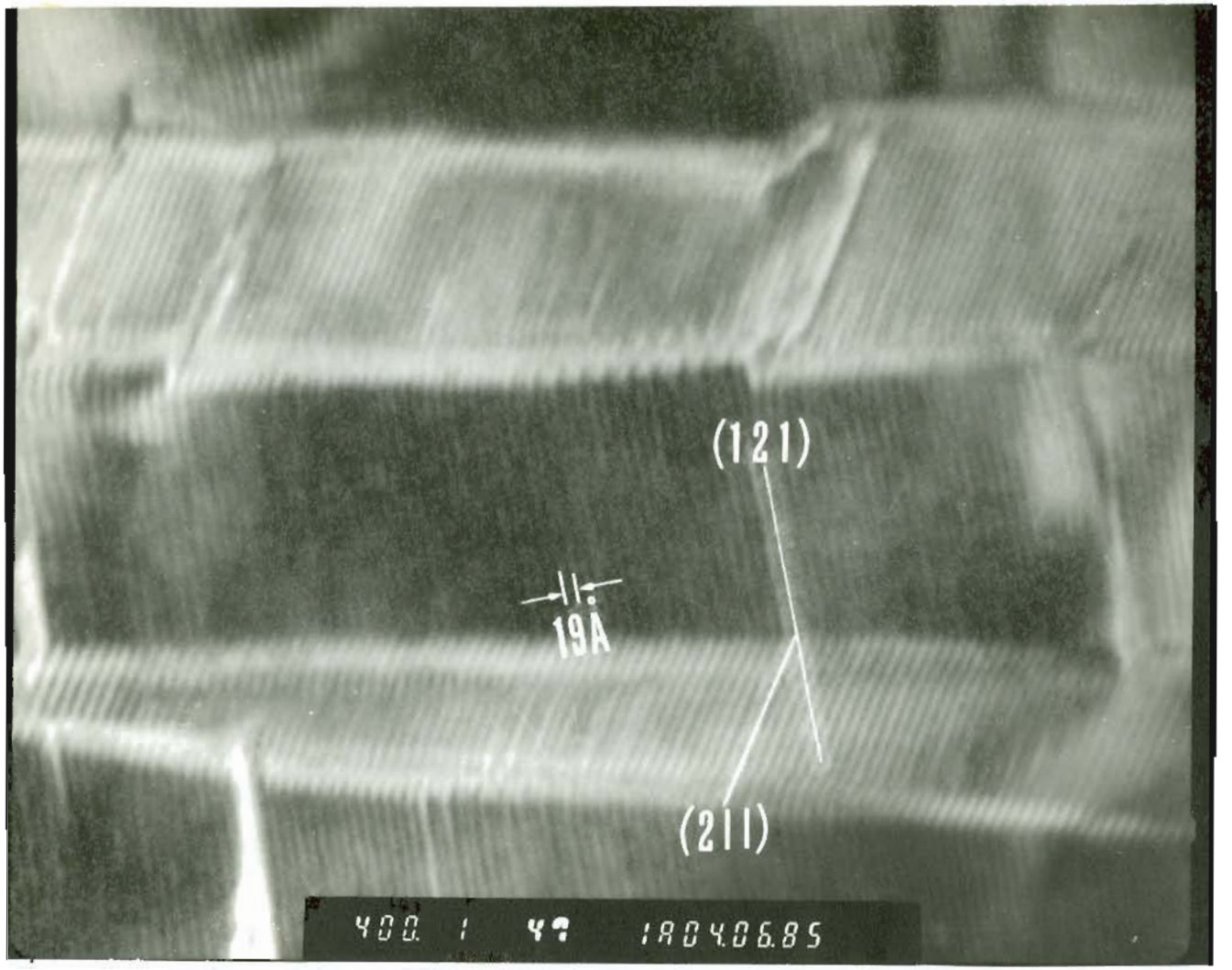

Fig. T-5. Higher magnification of CS planes {121} of doped sample reduced at 1100°C, $P_{O_2}=10^{-16.5}$ atm. (a); Zigzag lamellae of (121) and (211) CS planes, (b); $(2\bar{1}1)$ CS planes. CS spacing is 19Å in both.

(b)

8. CONCLUSIONS.

1. Nonstoichiometric, doped and undoped rutile, TiO_{2-x} exhibits two defect structure regions; a point defect region at comparatively high oxygen partial pressures and an extended defect region where point defects coexist before a homologous series of phases appear.

2. In the point defect region, the electrical conductivity of the undoped rutile is proportional to $P_{O_2}^{-1/6}$ at low temperature and changes to $P_{O_2}^{-1/5}$ at high temperature at very low oxygen activities.

3. The effects of low levels of Cr dopant as an acceptor on the electrical conductivity in a reducing atmosphere is negligible, except for a slight shift of the n-p transition to lower oxygen partial pressures.

4. The microstructure of the reduced crystals in the region of a sudden increase of conductivity contains {132} and {121}CS planar faults. The generation of these CS planes causes the abrupt increase of conductivity with reduction in the very low oxygen activities. The new reaction model of equations (28′) and (30′)

explains this particular behavior.

9.RECOMMENDATIONS FOR FUTURE WORK.

1.Thermogravimetric measurement of doped rutile during reduction/oxidation would enable the calculation of the x value in MO_{2-x}(M;sum of Ti and dopant). From these results, the density of the electron charge carrier can be calculated based on the assumption of a fixed unit cell for rutile. From the conductivity measurement, the charge carrier mobility can be obtained.

2.The counter effect of opposite dopants on conductivity and dielectric properties can be studied by simultanious doping of controlled amounts of donors and acceptors to study whether they simply compensate each other electronically as counterpartners or contribute other complex defects. The results will be useful in the control the effect of unintended impurities.

3.The effect of grain boundaries on the electrical conductivity of polycrystalline sample can be determined by controlling the grain size of test specimens. The conductivity measurements for different grain sizes will enable the quantitative analysis of grain boundary effect with the density and mobility of electron charge

carrier.

4. Reduced $BaTiO_3$ at very low oxygen activity shows similar dependence of conductivity to that of reduced rutile. (52) The study of microstructure of the reduced crystal may also lead to a new reaction model.

REFERENCES

1. F.A.Kröger and H.J.Vink,"Solid State Physics,"(Frederic Seitz and David Turnbull,Eds.) Vol.3.pp307-435, Academic Press, New York,(1956).
2. U.Balachandran and N.G.Eror,"Electrical conductivity in non-stoichiometric TiO_{2-x} at elevated temperatures" in press.
3. J.F.Baumard and E.Tani, J. Chem.Phys. Vol.67,No.3. 857(1977).
4. R.N.Blumenthal, J.Baukus, and W.M.Hirthe, J.Electrochem. Soc. Vol.114, No.2. 172(1967).
5. G.Levin and C.J.Rosa, Z.Metallkde, Vol.70,No.9. 601(1979).
6. G.Levin and C.J.Rosa, Z.Metallkde, Vol.70,No.10. 646(1979).
7. R.G.Breckenridge and W.R.Hosler, Phys.Rev. Vol.91,No.4. 793(1953).
8. R.F.Bartholomew, Phys.Rev. Vol.187,No.3. 828(1969).
9. J.H.Becker and W.R.hosler, Phys.Rev. Vol.137,No.6A,A1872 (1965).
10. J.F.Marucco, J.Gautron, and P.Lemasson, J.Phys.Chem. Solids, Vol.42, 363(1981).
11. R.R.Merritt and B.G.Hyde,and L.A. Bursill and D.K.Philp,

Phil.Trans.Roy.Soc.London, A 274, 627(1973).

12. K.S.Førland, Acta Chem.Scand.18, No.5,1267(1964).
13. R.T.Dirstine and C.J.Rosa, Z.Metallkde,Vol.70,No.6.372 (1979).
14. U.Balachandran and N.G.Eror, J.Mat.Sci.17, 1207(1982).
15. J.R.Akse and H.B.Whitehurst, J.Phys.Chem.Solids, Vol.39,457(1978).
16. J.F.Baumard, Solid State Comm. Vol.20, 859(1976).
17. D.C.Cronemeyer, Phys.Rev. Vol.113, No.5. 1222(1959).
18. J.F.Houlihan and L.N.Mulay, Inorganic Chem. Vol.13, No.3. 745(1974).
19. P.H.Zimmermunn, Phys.Rev.B. Vol.8,No.8. 3917(1973).
20. G.V.Chandrashekhar and R.S.Title, J.Electrochem.Soc. 392(1976).
21. S.Amelinckx and J.Van Landuyt,in "The Chemistry of Extended Defects in Non-metallic Solids"(Edited by L.Eyring and M.O'Keeffe),p295, North Holland, Amsterdam(1970).
22. J.F.Baumard, D.Panis, and A.M.Anthony, J.Sol.State Chem.20, 43(1977).
23. E.Tani and J.F.Baumard, J.Solid State Chem. 32, 105(1980).
24. K.S.Førland, Acta Chem.Scand. 18, 1267(1964).
25. R.T.Dirstine and C.R.Rosa, Z.Metallkde, Vol.70,No.5.

322(1979).

26. B.G.Hyde and L.A.Bursill, in"The Chemistry of Extended defects in Non-metallic Solids"(Edited by L.Eyring and M.O'Keeffe), p347,North Holland, Amsterdam(1970).
27. L.A.Bursill and B.G.Hyde, in "Progress in Solid State Chemistry,"(Edited by H.Reiss and J.O.McCaldin) Vol.7, p202,Pergamon, London(1972).
28. S.Amelinckx and J.Van Landuyt, in "Electron Microscopy in Mineralogy,"(Edited by H.R.Wenk) p68,Springer-Verlag Berlin Heidelberg(1976).
29. S.Andersson, Acta Chem.Scand.14. 1161(1960).
30. S.Andersson and L.Jahnberg, Ark.Kem.21, 413(1963).
31. L.A.Bursill, B.G.Hyde, O.Terasaki and D.Watanabe, Phil.Mag. 20, 347(1969).
32. L.A.Bursill and B.G.Hyde, Acta Cryst. B27, 210(1971).
33. N.G.Eror and D.M.Smyth, in "The Chemistry of Extended Defects in Non-metallic Solids,"(Edited by L.Eyring and M.O'Keeffe) p62, North-Holland, Amsterdam(1970).
34. C.Marcilly, P.Courty, and B.Delmon, J.Amer.Cer.Soc. Vol.53, No.1. 56(1970).
35. P.Deines, R.H.Nafziger, G.C.Ulmer, and E.Woerman, Bull. of the Earth and Mineral Sciences(Edited by College of Earth and Mineral Sciences),No.88, the

Pennsylvania State Univ.(1974).

36. L.S.Darken and R.W.Gurry, J.Amer.Chem.Soc. 67, 1398 (1945).
37. J.Yahia, Phys.Rev. Vol.130, No.5. 1711(1963).
38. H.J.Gerritsen, S.E.Harrison, H.R.Lewis and J.P.Wittke, Phys.Rev.Letters, Vol.2, No.4. 153(1959).
39. H.R.P.Frederikse, J.Appl.Phys. 32, 2211(1961).
40. J.Gautron, J.F.Marucco,and P.Lemasson, Mat.Res.Bull. Vol.16, 575(1981).
41. J.F.Houlihan, R.T.Dirstine,and D.P.Madacsi, Mat.Res. Bull. Vol.16, 659(1981).
42. P.F.Chester, J.Appl.Phys. 32, 866(1961).
43. F.A.Kroger, J.Phys.Chem.Solids, Vol.44, No.4. 345(1983).
44. C.R.A.Catlow and R.James, in "The Chemical Physics of Solids and Their Surfaces,"(Edited by M.W.Roberts and J.M.Thomas) Vol.8, Royal Society of Chemistry,London, 108(1980).
45. L.A.Bursill and B.G.Hyde, Phil. Mag. 23, 3(1971).
46. R.N.Blumenthal and D.H. Whitmore, J.Electrochem.Soc. Vol.110,(1963).
47. J.Van Landuyt, R.De Ridder, R.Gevers,and S.Amelinckx, Mat.Res.Bull. Vol.5, 353(1970).
48. J.Van Landuyt and S.Amelinckx, Mat.Res.Bull. Vol.5, 267(1970).

49. D.K.Philp and L.A.Bursill, Acta Cryst. A30, 265(1974).

50. R.R.Hasiguti, Annual Rev.Mat.Sci. 2, 69(1972).

51. R.M.Gibb and J.S.Anderson, J. Sol.State chem.4.379(1972).

52. Communication to Dr.N.Eror (Oregon Graduate Center)
by Dr.H.U.Anderson (Univ. of Missouri-Rolla)

APPENDIX 1.

VARIATION OF DONOR ACTIVATION WITH ITS CONCENTRATION AT CONSTANT TEMPERATURE.

When an n-type semiconductor containing Nd cm^{-3} of monovalent donor impurities is in thermal equilibrium, the fraction of ionized donors depends on doping concentration.

Effective density of states in the conduction band is

$$Nc = 2(2\, m_c kT/h^2)^{3/2} \quad \text{-----(a-1)}$$

If the Fermi energy E_f is lower than Ec, the free electron density is

$$n_o = Nc \exp[-(Ec-E_f)/kT] \quad \text{---(a-2)}$$

When the doping level is Nd and Ndi are ionized, then Nd-Ndi=Ndn are neutral. The ratio of (# of neutral/# of ionized state)

$$(Ndn/Ndi)=[Ndn/(Nd-Ndn)]=g \exp[(E_f+Ed-Ec)/kT] \quad \text{--(a-3)}$$

where g is the statistical weight of neutral state.

Suppose there are no other impurities and band tailing of the conduction band is neglected. Then n_o=Ndi=Nd-Ndn. From equation (a-2) and (a-3) the uncompensated carrier density satisfies

$$n_o^2/(Nd-n_o) = (Nc/g)\exp[-Ed/(kT)]=n_1 \quad ---(a-4)$$

Therefore,

$$n_o = n_1/2[(1+4Nd/n_1)^{1/2} -1] \quad ---(a-5)$$

The parameter n_1 determines how n_o/Nd varies with Nd for a given temperature by the following relation,

$$n_o/Nd = n_1/(2Nd)[(1+4Nd/n_1)^{1/2} -1] \quad ---(a-6)$$

The relation of equation (a-6) is numerically depicted in table and graph in the follwing page.

REFERENCE

J.S.Blakemore,"Semiconductor Statistics",Pergamon Press, Chapt.3,p117(1962)

N_d/n_1	n_o/N_d	n_o/n_1
0.001	0.999	0.001
0.003	0.997	0.003
0.01	0.990	0.010
0.03	0.972	0.029
0.1	0.916	0.092
0.3	0.805	0.242
1.0	0.618	0.618
2.0	0.500	1.00
4.0	0.390	1.56
6.0	0.333	2.00
8.0	0.297	2.37
10.0	0.270	2.70
12.0	0.250	3.00
14.0	0.234	3.28
16.0	0.221	3.53
18.0	0.2096	3.77

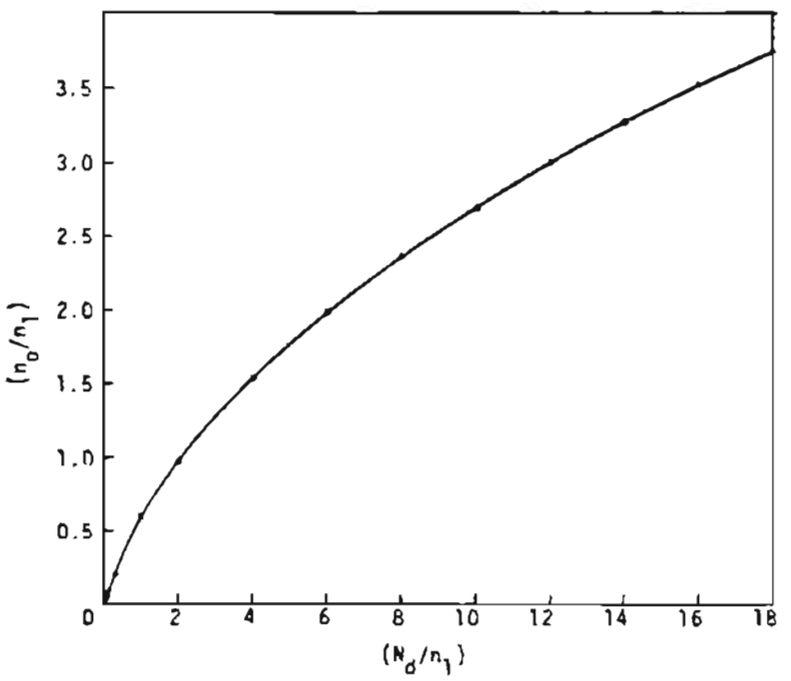

Table and Figure A: The relation between uncompensated carrier density, n_o vs donor density at a given temperature (that is a fixed value of parameter n_1).

APPENDIX 2.

VISIBILITY OF LATTICE DEFECTS IN T.E.M.

The amplitude of the scattered electron wave from a crystal as a whole is

$$\Psi \sim \int_{X\text{-tal}} \exp[2\pi i(g+s)*(r_n+R)]dt$$

where g is a vector of reciprocal lattice, s the deviation vector, r_n the position of unit cell with respect to the origin of the crystal, R the displacement vector for the defect, t thickness of the sample along the incident beam direction. $g*r_n$ is always an integer and s*R is very small compared to other terms, so it may be neglected. As a result, the scattered amplitude becomes

$$\Psi \sim \int_{X\text{-tal}} \exp 2\pi i[(g*R)+s*r_n]dt$$

For the case of a perfect crystal, the scattered amplitude is

$$\Psi \sim \int_{X\text{-tal}} \exp 2\pi i[(g+s)*r_n]dt$$

Thus, the scattered amplitude of a perfect crystal is modified by the phase factor $2\pi g \star R$ for the defect in the crystal. The phase factor gives a different intensity from the background intensity which comes from the perfect portion of the crystal. Therefore, defects may be visible. Accordingly, the magnitude of $g \star R$ must be sufficient to give a detectable contrast over the background.

Appendix 3.

The nature of the outer fringes in α- and δ- fringes.

α -fringes;

	Bright field		Dark field	
	First	Last	First	Last
$\sin\alpha > 0$	Bright	Bright	Bright	Dark
$\sin\alpha < 0$	Dark	Dark	Dark	Bright

$\alpha = 2\pi g*R$

δ -fringes;

	Bright field		Dark field	
	First	Last	First	Last
$\delta > 0$	Bright	Dark	Bright	Bright
$\delta < 0$	Dark	Bright	Dark	Dark

BIOGRAPHICAL NOTE

The author was born in Pusan, Korea, on 13 March, 1942. He received his B.S. degree in Physics from Seoul National University in 1964. He joined the Korean Air Force Army where he served for the next five years as weather forecast officer. Discharging from active duty of the army, he spent four years in teaching physics at high school before he came to the United States to pursue graduate studies. He received his M.S. degree in Materials Science from University of Utah in 1977, M.S. degree in Ceramic Science from Ohio State University in 1979. He joined the Materials Science Department of Oregon Graduate Center in 1979.

He completed the requirements for the degree of Doctor of Philosophy in Materials Science in 1984 and joined the Sintex Pacific Hard Metals Co. to do research of chemical vapor deposition of refractory compounds.

Currently he is postdoctoral research associate at Materials Science Department, carrying out research on capacitor materials and MOCVD of III-V compounds.